

Myth and Reality of a Universal Lithium-Ion Battery Electrode Design Optimum: A Perspective and Case Study

Daniel Witt, Dion Wilde, Florian Baakes, Fethi Belkhir, Fridolin Röder, and Ulrike Krewer*

The quest toward optimal electrode design for energy- and power-demanding applications involves besides experimental effort also less resource-intensive model-based studies. The diversity of optimization objectives and benchmark systems complicates the practical utilization of available methods and gained knowledge. Despite the increasing importance of fast charging, electrode design studies commonly focus only on discharge characteristics. This paper features, besides an overview and perspective of electrode structuring concepts and optimization pathways, a model-based full cell parameter screening of two-layered electrodes for charge and discharge. The small fraction of cells with superior performance among the evaluated configurations underlines the importance of a joint experimental and model-based electrode design optimization. The results further indicate that the performance of cell designs tailored for fast charge or fast discharge differs substantially; the gap widens if charging is terminated below 0 V versus Li/Li⁺ to prevent lithium plating. The broad parameter screening is complemented by a high-resolution half cell parameter study. Their comparison underlines that the benefit of electrode structuring depends heavily on the study extent and the chosen benchmark. Furthermore, the importance of the parameter space surrounding an optimal electrode design for production with process tolerances is highlighted.

1. Introduction

Lithium-ion batteries are an integral part of mobile energy-storage solutions, ranging from consumer electronics and power tools to automotive and future aeronautical^[1] applications. Although all these areas benefit from high energy density and low production costs of batteries, battery-powered vehicles are especially sensitive to these aspects due to their high capacity requirements. Apart from cost-saving process improvements like reduced solvent use in electrode production or a shortened cell formation time, an increased active material (AM) loading has the appeal of targeting production cost and energy density at the same time.^[2,3] A higher capacity per coated electrode area enables a higher production throughput, increases the ratio between AM and passive components like current collector and separator, and thus increases the theoretical volumetric capacity of a cell. On the downside, a plain increase in the coating thickness without modifying further electrode parameters can significantly

limit the current rating of a cell, as shown in **Figure 1a**. To overcome this poor C-rate capability, a broad body of literature elaborates on both production process and electrode design advancements. The required insight to move from a trial-and-error approach to a knowledge-driven electrode optimization is given by physicochemical models. They can aid in the understanding of limiting processes in cells with thick electrodes, e.g., by revealing electrolyte deprivation at high C-rates (see **Figure 1b**).

Literature provides a wide range of experimental and model-based approaches toward optimal electrode design for improved energy densities and performance characteristics. **Figure 2** shows an overview of possible pathways toward optimal electrode design. As a general rule, the first step toward any optimization problem should be the clear definition of an optimization objective along with a corresponding benchmark system that enables a meaningful evaluation of the optimization progress. In case of multiple target criteria, the optimization problem may be extended to combine multiple objectives like volumetric capacity and aging optimal as well as lithium plating-free fast charge capability. In the next step, state-of-the-art and novel cell design options must be evaluated with respect to their relevance to the optimization problem. Here, simple approaches like an

D. Witt, D. Wilde, F. Baakes, Prof. U. Krewer
Institute for Applied Materials-Electrochemical Technologies
Karlsruhe Institute of Technology
Adenauerring 20b, Karlsruhe 76131, Germany
E-mail: ulrike.krewer@kit.edu

D. Witt, Dr. F. Belkhir, Prof. F. Röder
Institute of Energy and Process Systems Engineering
TU Braunschweig
Langer Kamp 19b, Braunschweig 38106, Germany

D. Witt, Dr. F. Belkhir, Prof. F. Röder
Battery LabFactory Braunschweig
TU Braunschweig
Langer Kamp 8, Braunschweig 38106, Germany

 The ORCID identification number(s) for the author(s) of this article can be found under <https://doi.org/10.1002/ente.202000989>.

© 2021 The Authors. Energy Technology published by Wiley-VCH GmbH. This is an open access article under the terms of the Creative Commons Attribution License, which permits use, distribution and reproduction in any medium, provided the original work is properly cited.

DOI: 10.1002/ente.202000989

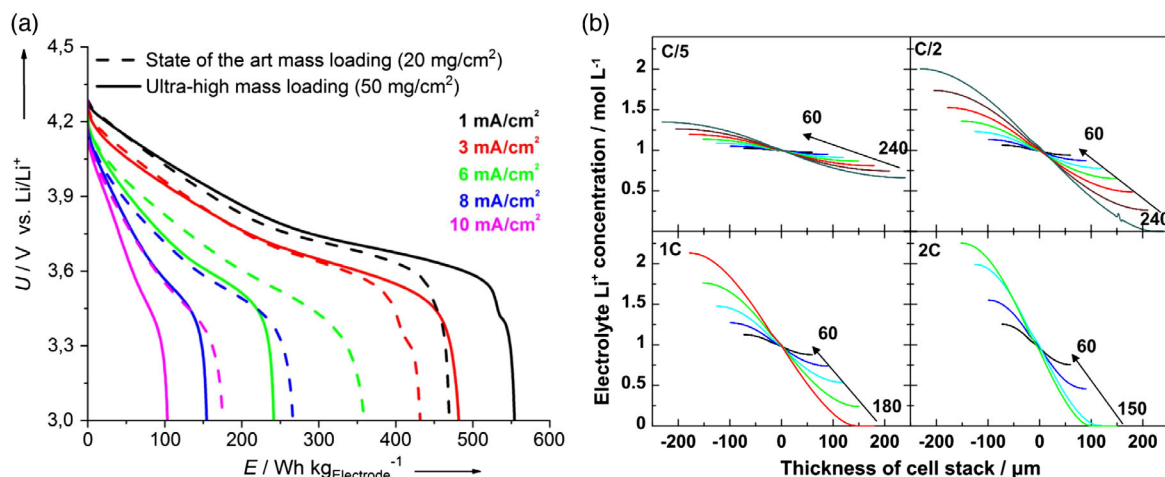


Figure 1. a) Experimentally recorded cathode half cell potential versus specific energy of two NMC622 cathodes with a state-of-the-art mass loading (3.2 mAh cm^{-2}) and an ultra-high mass loading (8 mAh cm^{-2}). Reproduced with permission.^[22] Copyright 2019, John Wiley and Sons. b) Simulated lithium-ion concentration profiles in the electrolyte phase between anode (left) and cathode (right) across a cell at the end of discharge for different electrode thicknesses and at different C-rates. Reproduced with permission.^[102] Copyright 2017, Springer Nature.

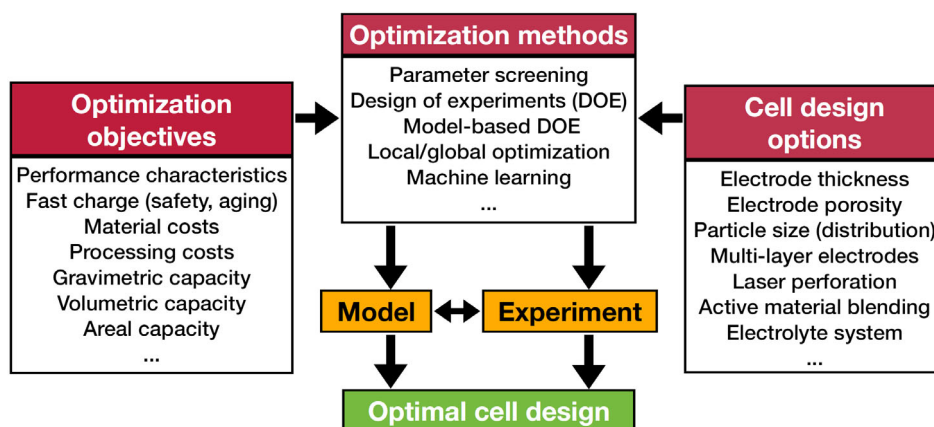


Figure 2. An overview of possible optimization objectives for lithium-ion batteries along with possible cell design options and optimization methods. To arrive at an optimal cell design within this parameter space, either a battery model (physicochemical or data-driven), an experiment, or a synergistic combination of both can be used.

adjustment of the electrode thickness may be considered individually or combined with a variety of other structuring approaches like electrode grading or laser perforation. Finally, an optimization method must be chosen, in which then also the optimization objective and the selected cell design methods are integrated. Here, a fine-grained equidistant screening of a broad parameter space will likely be too expensive and time-consuming from an experimental and potentially also from a modeling perspective. For this reason, methods for an efficient exploration and exploitation of the parameter space like design of experiments (DOE) or direct mathematical optimization are crucial. To achieve an optimal utilization of available resources, a special focus should be on the synergistic combination of both approaches, e.g., via iterations between model prediction and experimental validation.

Despite the wide range of possible optimization objectives, electrode design is commonly regarded in the context of improved discharge characteristics. Although a broad body of

literature elaborates on challenges of fast charging,^[4–6] the focus commonly is not on optimal cell design for fast charging but rather aspects like favorable material properties,^[7–10] charging protocol optimization,^[11–14] cell aging,^[15–18] and temperature-related lithium-plating mitigation strategies.^[19,20] Some studies take into account the effect of electrode structure on lithium plating. Tanim et al. highlight the importance of low production tolerances for structural properties like electrode composition, porosity, and tortuosity to avoid an early onset of cell aging due to local electrode inhomogeneities.^[15] Vishnugopi et al. investigated the interrelation between electrode porosity, performance, and lithium plating at various temperatures.^[21] In contrast to electrode design optimizations for discharge, a basic study on ideal electrode design for both charge and discharge is yet unavailable in literature.

The heterogeneity of experimental and model-based studies with a diversity of optimization objectives and benchmark

systems complicates the selection of the best suitable electrode design concept for a specific application. Furthermore, electrode design studies commonly focus exclusively on discharge characteristics despite the increasing interest in fast charging. The goal of this work is to provide a perspective on electrode design for both discharge and charge operation. For this purpose, the work is divided into two major sections. In the first part, a broad overview and critical analysis of published electrode design concepts, battery models for electrode design, and optimization approaches is provided. It is concluded with a brief perspective on the overall challenges and opportunities in the field of electrode design optimization. The second part contains original research work and features two model-based case studies. The first study investigates the performance characteristics of full cells with a high theoretical capacity of 5 mAh cm^{-2} at different C-rates for charge and discharge. To provide a differentiated perspective on the mass transport limitation in thick electrodes, two-layered electrodes are investigated via a broad parameter screening with more than 5000 evaluated cell configurations. The second study focuses on a two-layered cathode half cell. This fine-grained parameter study is essentially a brute-force optimization that provides valuable insight into the importance of the parameter space surrounding the identified optimal electrode design. Both studies are compared, and recommendations are deduced.

2. Pathways toward Optimal Electrode Design

In this section, the possible pathways toward optimal electrode design in Figure 1 are discussed in more detail. First, fundamental electrode design concepts from experimental and model-based half and full cell studies are summarized to illustrate the diversity and combinatorial complexity of electrode design. Reported benefits of electrode design studies are critically assessed. Second, an overview of the range of battery models is given that aid in the understanding of limiting processes within a cell and support the experimental design of optimal lithium-ion battery electrodes. The third part begins with a critical discussion of possible optimization objectives and corresponding benchmark systems that inherently complicate the comparison of studies even with only a slightly different focus. Furthermore, it provides an overview of methods that can aid in the quest for optimal electrode design. In the last part, we provide a perspective on opportunities and challenges of electrode design optimization.

2.1. Electrode Design Concepts

Tailoring the design of electrodes to specific application requirements is a complex matter. This is related especially to the large variety of modifiable structure parameters and possible electrode structuring concepts. Besides increasing the coating thickness, the adjustment of the electrode porosity as well as the average particle radius are among the most prevalent ones.^[22–26] The paragraph below will address these concepts in the following order: porosity, average particle size, particle size distribution, and layer thickness.

Schmidt et al. studied the influence of different porosities for lithium nickel manganese cobalt oxide (NMC) cathodes.^[24] It

could be shown that decreasing the porosity from 50% to 25% leads to an increase in both volumetric energy and power density. Further decreasing the porosity to 18% increased the power density, but it decreased the energy density. Thus, a clear trade-off between these two optimization objectives can be observed. Similar results have been shown by Laue et al.^[27] Their study revealed that the capacity after calendaring shows a maximum at intermediate porosities for C-rates above 1C. Buqa et al. investigated the influence of different average particle sizes in graphite-based anodes on their rate capability during charge.^[23] The results show a clear advantage of small average particle sizes. When compared with large particle sizes ($D_{50} = 17 \mu\text{m}$), the smaller particle size sample ($D_{50} = 3.3 \mu\text{m}$) featured a 30% reduced capacity loss at a C-rate of 3C. Röder et al. have shown in a simulation study that the performance of a graphite-based anode with large particles differs significantly from an anode with a particle size distribution of large particles.^[28] In an experimental study, Bläubaum et al. concluded further that a narrow particle size distribution of neither small nor large particles is a good choice for graphite-based anodes due to higher solid electrolyte interphase-related degradation of small particles and a tendency toward lithium plating of large particles.^[29] Thus, a narrow distribution of medium-sized particles is suggested. In a comprehensive model-based and experimental study, Yu et al. have shown that the areal capacity can be increased by 23% at 1C by increasing the cathode thickness from 90 to 110 μm .^[30] However, they have also shown that further increasing the electrode thickness leads to a decline in areal capacity, indicating mass transport limitations. Similar results have been reported by several other studies.^[22,23]

The examples given above are appealing due to their comparably simple implementation. They could be realized with established production processes. However, electrodes optimized for high capacity may still suffer from poor rate capability due to transport limitations. To overcome these limitations, more elaborate methods have been developed. One idea to mitigate mass transport limitations within thick electrodes is the creation of new diffusion pathways. A prominent approach for this purpose is laser structuring. For instance, Habedank et al. treated electrodes with a laser to create new macropores by ablation of small fractions of the electrode coating.^[31] With this treatment, the discharge capacities for C-rates above 1C could be increased by 20% when compared with their unstructured counterparts. Smyrek et al. used laser structuring to introduce channels into NMC electrodes, resulting in a chessboard-pattern.^[32] With this approach, they increased the capacity retention at 3C about 30% when compared with the original unstructured and uncalendered electrode. When compared with a calendered electrode, the benefit of structuring was reduced, but it was still significant with roughly 15%. In other studies with several different cathode chemistries, similar results could be achieved.^[33,34]

All electrode design concepts discussed so far are based on electrodes consisting of one single layer. The structure of an electrode is not explicitly altered over its thickness. In recent years, the idea of multilayered electrodes surfaced. For example, Golmon et al. conducted a simulation study and reported an improvement of up to 61% in areal capacity compared with an unstructured electrode by optimizing for continuous porosity and particle radius profiles throughout the anode and cathode

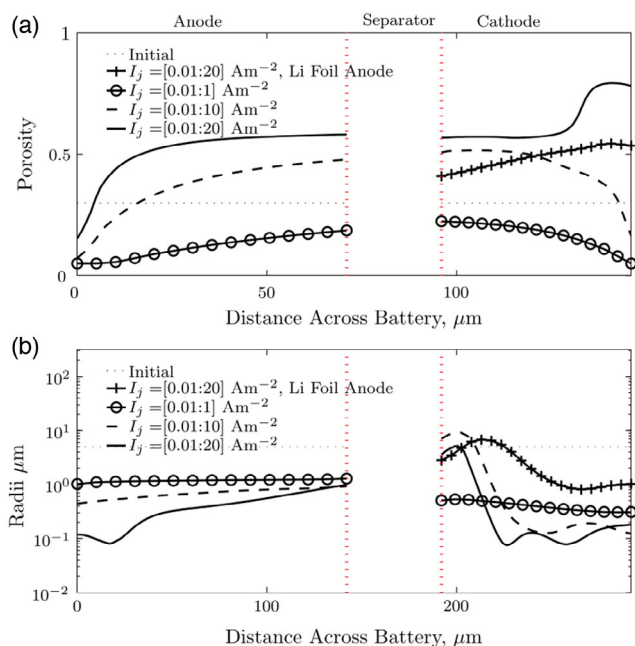


Figure 3. Initial and optimized local a) porosity and b) particle radius in a full cell setup for highest areal capacity with respect to different maximal C-rates. For the third-to-fifth legend entry, the theoretical capacities (and estimated maximal C-rate range) are approximately 3.8 mAh cm⁻² (C/30), 2.6 mAh cm⁻² (C/3), and 1.8 mAh cm⁻² (1C). The additional line with crossmarkers in the cathode region represents the optimal design with a lithium metal instead of a graphite anode. Reproduced with permission.^[35] Copyright 2013, Elsevier.

(see Figure 3).^[35] Recently, the experimental production of multilayered electrodes with different structural properties such as porosity, average particle radius, and layer thickness received attention with a patent.^[36] Nonetheless, there are also challenges due to the increased process complexity. Furthermore, increased electric losses at the interface between the two layers within an electrode were observed.^[37] Eventually, the benefit of structured electrodes must outweigh both their higher production complexity and production costs as well as surpass the characteristics of state-of-the-art electrodes to realize an economic production.

The following paragraph covers studies in which one or multiple of the aforementioned design parameters was explicitly optimized to obtain a better cell performance. Most of these studies contemplate half cells only.^[38–41] For instance, Chen et al. conducted a model-based study on heterogeneous cathode structures.^[41] They achieved a gravimetric energy density of 323.5 Whkg⁻¹ at 3C and conducted an internal comparison of the investigated electrode structures. A similar study by Ramadesigan et al. reported a possible decrease of ohmic resistance of up to 33% by applying a porosity gradient to a lithium cobalt oxide cathode.^[40] Here, the results were compared with an optimized homogeneous electrode. Dai et al. converted this less-tangible ohmic resistance reduction into an estimated 3% capacity increase.^[42] In a recent study, Qi et al. also optimized a cathode for reduced resistance.^[38] However, they reported only a 4.4% resistance reduction.

When comparing these advantages to full cell optimization studies, the reported improvements are in different orders of magnitude, depending on model assumptions and especially benchmark systems. For example, De et al. could demonstrate an increase in energy density of roughly 15% for discharge at 0.1C and around 66% at 6C.^[43] Here, the porosity and layer thickness of a homogeneous anode and cathode were chosen as design parameters. The benchmark was chosen arbitrarily. As already stated earlier, a 61% improvement in areal capacity could be achieved by Golmon et al. compared with an unstructured electrode by optimizing for continuous porosity and particle radius profiles over the thickness of the electrode (see Figure 3).^[35] In contrast, Dai et al. compared a full cell setup with varying cathode porosity over the electrode thickness, i.e., a discrete multilayered electrode, with an optimized single-layered electrode with constant porosity.^[42] They observed only a 3% improvement in energy density.

The strong deviations in the predicted optimization potentials with structured over homogeneous electrodes for both half cell and full cell studies highlight the challenge to extract useful information from electrode design studies. As already pointed out by several previous studies, the chosen optimization objective and benchmark system have an undeniable effect on the identified optimal electrode structure and its predicted benefit.^[24,42,43] As the chosen benchmark was different in each presented publication, mostly no tangible comparison can be made between them. Furthermore, benchmarks are often arbitrarily chosen, which further complicates the comparison of different studies. However, there are also some studies that used optimized homogeneous electrodes as a benchmark for a more general assessment of the benefit from electrode structuring.^[40,42]

2.2. Models for Optimal Electrode Design

Overall, the matter of designing electrodes for a specific application is an intricate one. Considering the broad range of electrode design concepts and their possible combinations, identifying the best suitable one experimentally seems to be at least a costly and time-consuming, if not unsustainable, approach. Here, physicochemical models can help to gain an understanding of the merits and limitations of specific electrode structuring concepts before extensive experimental work is done. In the following, a brief overview of the most relevant battery models for the study of electrode structuring is provided. A special focus will be on those models that are computationally suitable for both rapid screening of electrode design concepts and mathematical electrode structure optimizations. The model overview begins with the computationally most efficient models, advances to more complex ones, and ends with approaches that make insights from complex models available to computationally less-demanding ones.

Empirical models use mathematical functions with empirical coefficients. Here, functions and parameters do not have a direct physical meaning. They are rather modified to reproduce experimental data. Such models usually have low computational cost and allow for fast simulations. However, these models are only valid in the range of the underlying training data. This makes them useful for applications like monitoring the state of charge of a battery within battery management systems^[44,45] but not so

much for predictions beyond the cell chemistry and cell design that was used for parameterization.

Electrochemical engineering or physicochemical models use mechanistic equations to describe processes like diffusion, conduction, migration, and electrochemical reaction kinetics. They provide an in-depth physical insight into the effect of structural parameters on limiting processes within electrodes. These models enable an extrapolation to cell designs different from the experimental cell design used for model parameterization and validation. The simplest representative of this modeling type is the single particle model (SPM), in which a single particle represents a whole electrode. This model may be used for structure optimization, as already done for the investigation of different particle size distributions.^[28] However, its application is limited to thin electrodes investigated at low C-rates.^[46] It is less useful in the context of designing high-capacity electrodes as it does not take into account potential and concentration changes in the solid and electrolyte phase throughout the electrode.

The more complex pseudo-2D (P2D) battery model is based on porous electrode theory and concentrated solution theory. It was originally developed by Doyle et al.^[47] The simulation of one discharge curve is already more expensive compared with the SPM, but it is still in the range of minutes or even seconds. Like the SPM, it assumes homogenized electrodes, but it enables a spatial discretization of the homogenized electrode into multiple representative particles along with corresponding electrolyte volume elements over the thickness of the electrode. Thus, it can provide insights into local concentrations and potentials in both the solid and the electrolyte phase. At the same time, the higher discretization level enables a more accurate representation of dynamic measurements. This is commonly achieved without directly considering the microstructure of the electrodes. For instance, pore connectivity as a function of AM, carbon black and binder volume fraction, and particle size is mostly neglected. Such structural information is typically incorporated into lumped parameters like the effective electric conductivity or the tortuosity. To analyze the effect of spatial inhomogeneity of the electrode structure on cell performance, the P2D model has received numerous extensions for the investigation of porosity gradients in electrodes,^[40,42] different particle sizes and particle size distributions,^[25,48–50] and also a combination of both.^[35] The model has already been used for a wide range of studies in the field of electrode design. For instance, it was used for the identification of the most sensitive model parameters for cell performance.^[51,52] Colclasure et al. conducted a parameter study with thick electrodes and identified transport in the electrolyte phase as the limiting process and proposed required electrolyte properties to overcome this limitation.^[8]

3D microstructure-resolved battery models add another level of detail as they directly utilize electrode microstructures.^[53] These structures can be created virtually by microstructure generators^[54,55] or can be acquired experimentally by either X-ray tomography,^[56–58] focused ion-beam scanning electron microscopy,^[59,60] or a combination of both.^[61] A further analysis of these microstructures can provide quantitative information on particle size distributions, surface areas, volume fractions, and surface areas for the AM phase, carbon black-binder phase, and pore phase.^[62,63] In 3D microstructure simulations, electrolyte and AM concentrations and potentials can be resolved throughout

the whole cell. Although computationally much more demanding than a P2D model, possible applications for these 3D models are extensive. For instance, they can be used to evaluate existing structuring concepts or identify thermal hotspots and local lithium plating.^[64–66] Kespe et al. used 3D microstructure simulations to improve the electric conductivity of an electrode by optimizing the spatial location of the carbon-binder domain (CBD).^[67] Chouchane et al. looked at the CBD from a production perspective.^[68] Based on manufacturing simulations, they predicted the effect of the spatial location of the CBD on cell performance. Duquesnoy et al. proposed a data-driven methodology that facilitates the analysis of the interdependencies between calendaring process parameters and final electrode properties by combining experimental data, in silico mesostructure generation, and machine learning.^[69] A complete structural optimization has been done by Mitchell et al.^[70] They mathematically optimized the topology of a silicon anode microstructure for maximal electric conductivity and minimal electrode volume expansion.

To circumvent the—at least at present—significant computational effort of 3D microstructure simulations, there have been efforts in the literature by Mistry et al.^[71] and Laue et al.^[27,72] to combine the rather moderate computational effort of the P2D model with polynomials that capture the effect of an electrode microstructure on effective transport parameters within the P2D model. For this purpose, Mistry et al. virtually created microstructures to derive effective microstructure-related polynomials of tortuosity, conductivity, and AM surface area. Laue et al. investigated the representation of microstructure properties in the P2D model for a calendaring study on NMC cathodes.^[27] The starting point was a stochastic 3D microstructure simulation from which they derived effective polynomials that are physically motivated. **Figure 4** shows a comparison of these polynomials with the Bruggeman approach. It underlines that the empirical polynomial captures the effect of the percolation threshold on the electric conductivity, whereas the Bruggeman approach clearly cannot. Furthermore, Laue et al. derived an effective polynomial for the active surface area of the cathode that captures the decline of this parameter for very low and very high solid volume fractions. Eventually, the utilization of these 3D microstructure-derived

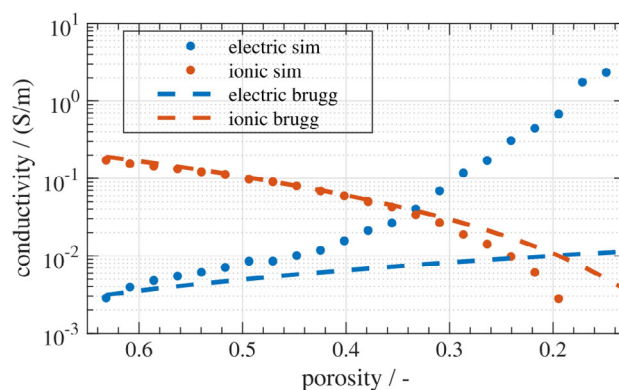


Figure 4. A comparison of predicted effective electric (blue) and ionic (orange) conductivity versus porosity for two modeling approaches: 3D microstructure simulation (dots) and Bruggeman relation (dashed lines). The AM-to-carbon black volume ratio is kept constant at 4.4/1. Reproduced with permission.^[27] Copyright 2019, Elsevier.

polynomials considerably extended the prediction capability of the P2D model to electrodes with different calendaring degrees while preserving its rapid simulation capability. However, without a comparison with experimental microstructure reconstructions, the stochastic microstructure generation leaves some uncertainty in the derived polynomials.

2.3. Optimization Approaches

The previous part of the literature survey highlighted the difficulty to compare reported improvements of different electrode design concepts. The diversity of optimization objectives along with the corresponding broad range of reasonable benchmark electrodes is an inherent consequence of the variety of possible application requirements. Published studies on electrode design just mirror this diversity and illustrate its complexity. In the following paragraphs, the topic of optimization objectives as well as corresponding benchmark systems is discussed in more detail as it lays the foundation for the solution of any design problem. Subsequently, available optimization methods are presented that enable the translation of an objective into an optimal electrode design.

In general, a universal formulation of an electrode design problem is everything but straightforward. Depending on the desired application, the focus could be on the performance characteristic of a cell at a given C-rate or over a specific C-rate range.^[73] The targeted performance characteristic may be the areal capacity,^[22,30,35] the gravimetric^[22,42] or volumetric energy density,^[24,42] or even the volumetric power density.^[24] Other targets may comprise a minimum mean overpotential in an electrode along with a minimum spatial deviation from its mean value, which would result in a more homogeneous mechanical stress throughout the electrode.^[38] Obviously, this list of optimization objectives does not aim to be comprehensive due to the variety of possible application scenarios. However, there are a few fundamental aspects of quantifying performance that have to be discussed. In a first step, these are areal, volumetric, and gravimetric metrics. In a second step, the difference between capacity, energy, and power will be discussed.

Areal metrics like the areal capacity are the most unambiguous and intuitive performance measures due to their independence of coating thickness and mass or volume of passive materials like separators and current collectors. In contrast, volumetric and gravimetric metrics require a precise definition of the considered materials within the cell. If one study investigates the capacity per AM mass, and another study provides the capacity per total electrode mass, the results are hardly comparable without additional information. However, with different optimization objectives like high AM utilization or a mass-constrained application, both definitions are reasonable.

As a performance metric, the capacity is universally applicable to the investigation of charge and discharge. If the energy density was chosen as an evaluation metric, a high energy density during charge could either indicate high ohmic losses, i.e., a low charging efficiency, or a high charged capacity. However, this is also the strength of the energy density as it enables the assessment of the energy conversion efficiency due to the consideration of both voltage level and capacity. Power characteristics may be seen as a different category as they combine energy density and rate

capability. This is crucial, e.g., in the context of electric vehicles with a high discharge power demand for acceleration and a high charge power requirement for maximal recuperation of kinetic energy during deceleration. On the downside, the power density does not enable an assessment of the actually usable capacity or energy. In the end, at least one performance metric must be chosen to enable an optimization.

Similar to the universal definition of an optimization problem for all application scenarios, the question for the one true single-layered benchmark electrode simply cannot be answered. Depending on the optimization objective, different benchmarks are required to enable an unbiased evaluation of the optimization progress. In this context, the utilization of arbitrary benchmark systems seems unfavorable but especially for experimental studies likely unavoidable due to the large design parameter space. A more general assessment of the merits and limitations of an electrode design concept would require an optimized state-of-the-art benchmark electrode. From the perspective of electrode production, this would help to answer the question if the necessary process development and equipment establishment for a structured electrode are well invested. The earlier discussed work by Dai et al. highlighted this aspect by comparing an optimized homogeneous electrode with an optimized electrode with varying porosity at multiple C-rates.^[42] Their estimated benefit from electrode grading was relatively small compared with studies with nonoptimized benchmark electrodes. As a result, a study without an optimized benchmark can only estimate trends within the investigated parameter space. With an optimized benchmark, a more general evaluation of an electrode design concept becomes possible.

The most basic approach to solve an optimization problem is an experimental parameter screening. Considering the required equipment, personnel costs, and operational costs, such experimental studies most likely have to focus on the estimation of a local optimum. A battery model that is validated over a wide range of measurement data can go beyond local optima and approximate the global optimum, using global mathematical optimization algorithms like particle swarm optimization, genetic algorithm, and Bayesian optimization.^[74] Here, the latter method can additionally provide confidence intervals for the optimized parameters, enabling a first evaluation of parameter sensitivity and interrelation.

Even without a battery model, an equidistant experimental parameter screening may not be necessary. With DOE, a statistics-based minimum scope of experiments can be defined that still allows for the reconstruction of the interrelation between the optimization target and the chosen design parameters. For instance, Su et al. used DOE for the identification of the most relevant factors for capacity degradation in lithium-ion batteries.^[75] Rynne et al. developed a guideline for the application of DOE to the problem of electrode formulation.^[76] A further reduction of required experiments may be achieved via model-based design of experiments (MBDOE). It is commonly used for the definition of experiments that are best suitable and most efficient for parameter identification.^[77–80] In contrast to the purely statistics-based DOE, MBDOE enables a knowledge-based definition of the most insightful experiments before any experimental study is conducted.

Especially in the field of material design and discovery, model-based high throughput instead of mathematical optimization

approaches are used to identify the best possible solution within a broad parameter space.^[81,82] For example, this has been done extensively with density functional theory simulations for applications like solid-state lithium-ion conductors.^[83,84] To the best of the authors' knowledge, there are no experimental studies on high-throughput lithium-ion battery electrode design, comprising both highly adaptable electrode production and electrochemical characterization. In contrast, model-based studies are limited primarily by their validity range and only secondarily by the available computational resources.

Machine learning is another approach to improve the understanding and eventually enable an optimization of process parameters for their effect on the final electrode properties. Such data-driven models can correlate large amounts of input data like process parameters or electrochemical characterization data with output data, such as performance or aging characteristics. This is especially valuable if a good physical understanding of the underlying processes is yet unavailable. In general, data-driven approaches are an option, especially if high-quality data are already available or can be generated easily. For instance, Cunha et al. used machine learning algorithms for the investigation of the interrelation between slurry manufacturing parameters and final cathode mass loading and porosity.^[85] Considering electrode design-specific aging characteristics, data-driven approaches may also help to extend the scope of electrode design and manufacturing optimization to battery aging. In the context of cell characterization, Severson et al. used machine learning for the prediction of battery lifetime based only on the first few aging cycles.^[86] Attia et al. conducted a closed-loop optimization of fast-charging protocols by iteratively defining the next experiments based on a data-driven lifetime prediction model.^[12] Nonetheless, physicochemical models remain essential for the understanding of underlying physical processes. They can provide knowledge on internal and not directly measurable states that aid in the identification and mitigation of limiting processes. In a slightly different context, a machine learning-based surrogate model was created from a P2D model to enable a fast end-of-line cell characterization.^[87] This kind of surrogate modeling could also help to reduce the computational effort of physicochemical battery models for electrode design optimization. Merits, limitations, and perspectives of the combination of physicochemical modeling with machine learning are discussed in detail by Dawson-Elli et al.^[88]

Recent work by Schmidt et al. investigated the effect of production tolerances on final product properties.^[89] With a Monte-Carlo approach, a large number of cell configurations was sampled from the probability distributions of different production tolerances, for instance, regarding electrode porosity or thickness. Here, different parameter sensitivities lead to an uneven performance distribution especially at high C-rates due to more pronounced voltage losses.^[89,90] From an electrode design perspective, this puts emphasis on the necessity to consider production tolerances for the design of electrodes. Robust optimization can help to identify a cell design that delivers similar performance characteristics despite uncertainties in the production process. To the best of the authors' knowledge, the application of robust optimization to the problem of electrode production is yet unavailable. However, in the context of process engineering, efficient frameworks for robust optimization have already been established.^[91,92]

2.4. Opportunities and Challenges of Electrode Design Optimization

Researchers in the field of electrode design are blessed with a wide range of electrode design concepts. Furthermore, most concepts could be or already have been investigated with physicochemical battery models. For instance, 3D microstructure models can be used to investigate the effect of structural inhomogeneities on cell performance or even local lithium plating. P2D modeling approaches lack this detailed local insight but are computationally less expensive while enabling a reasonably accurate representation of experimental data. However, considering the rapid improvement of available computational resources, it may soon be practical to include 3D models into mathematical optimization routines.

Apart from physicochemical battery modeling, machine learning revealed itself as a valuable tool that facilitates the understanding and thus optimization of complex interrelations between process parameters and final cell properties or rather performance. Applications range from slurry production for electrode coating over electrode calendaring to aging prediction. Considering the importance of battery lifetime, a data-driven aging and performance prediction based on production process parameters seems highly relevant for process optimization. We further believe that future studies on electrode design should make uncertainties a fundamental part of the optimization process to enable not only superior performance characteristics but lay the foundation for an economic and more sustainable electrode production. Large experimental screening studies would likely be too expensive when compared with a direct optimization of a well-validated battery model. Without experiments, currently, neither the model can be properly parameterized, nor can the resulting model-based design recommendation be verified. However, the combination of production process understanding and battery modeling provides all the knowledge and tools to enable a rapid electrode design optimization.

Despite the broad coverage of electrode design in literature, the selection of the best suitable electrode design for a specific application is everything but straightforward. Different study objectives and often arbitrary benchmark systems complicate the comparison between studies and conceal the benefit of one studied electrode design for another application. However, some studies recognized this problem and used optimized benchmark systems. We believe that this is a step in the right direction. A model-based design optimization can support an experimental study by providing a prediction for such an optimal benchmark electrode. Nonetheless, different application requirements and thus optimization objectives will inevitably complicate the comparison between different studies. The choice of a benchmark system that is tailored toward the optimization objective and thus unbiased with respect to the study outcome can lay a sound foundation for better comparable results. Furthermore, it seems critical to provide not only the investigated performance characteristic but also the context for the derivation of other performance characteristics that may be more relevant to other application scenarios.

Finally, estimated design advantages from half cell studies should be interpreted with caution. The neglected interaction

with a realistic counter electrode may distort the achieved improvements. Concentration profiles throughout an electrode are likely to be less favorable with a state-of-the-art porous composite electrode instead of a lithium metal counter electrode.

3. Case Study: Model-Based Optimization of Two-Layered Electrodes

As shown in the first part of this article, electrode optimization can resort to a plethora of design concepts for the fulfillment of specific application requirements. For the investigation of these concepts, physicochemical battery models are available with various levels of detail, ranging from simple SPMs to microstructure-resolved simulations that enable a differentiated local assessment of limiting processes within an electrode. Considering the computational resources commonly available today, the long-established and extensively used P2D model nowadays still seems to offer the best compromise between model fidelity and computational effort. Consequently, the two case studies in this work make use of a P2D model, which is upgraded with insights from 3D microstructure simulations and is extended for two-layered electrodes to enable a broad electrode design screening with insightful structuring trends.

As discussed earlier, studies on electrode design commonly focus on discharge performance while using a wide range of benchmark systems. In the following section, two model-based electrode design studies are defined to create a better understanding of cell designs for charge and discharge, respectively. The first model-based study resembles an experimental parameter screening for a full cell setup with two-layered electrodes. It investigates general design principles for discharge and charge operation at various C-rates and whether they differ from each other. Here, the influence of the scope of a study and its benchmark on the study outcome is investigated. However, ten design parameters in this first study allow only for a coarse screening. Therefore, we choose as the second case study a fine-grained parameter variation for a two-layered cathode half cell in a significantly constricted parameter space. With only two design parameters, it provides a perspective on the importance of the scope of a study for both its outcome and its implied benefit from electrode structuring. Furthermore, with the potential economic and ecological impact of robust electrode production in mind, the high resolution of the parameter space allows for an evaluation of the relevance of production uncertainties in the context of electrode design.

3.1. Model Setup and Parameterization

For all studies in this work, the P2D model by Doyle et al. is chosen as a starting point to enable broad parameter variations with reasonable computational effort.^[47,93] Due to the importance of the electrode microstructure for the solid-phase electric conductivity and the mass transport through the electrolyte phase in the pore volume, empirical polynomials from 3D microstructure simulations from Laue et al. are used to integrate knowledge on the microstructure–parameter relationships into the homogenized but fast P2D model.^[27] The combination of these two modeling approaches has been successfully done in our prior

work for the investigation of the effect of the calendaring process on cell performance.^[27] This model lays the foundation for all studies in this work. The governing model equations for solid diffusion, solid as well as electrolyte potential, and electrolyte diffusion and migration are shown in **Table A1** in the Appendix. In contrast to the original P2D model by Doyle et al., this model considers an electrochemical double layer according to Legrand et al. to enable an accurate representation of the transition between different loads.^[94] The reaction kinetics are described with a Butler–Volmer equation and a constant exchange current density.

To enable the simulation of multilayered electrodes, the basic model is extended. The schematic full cell structure in **Figure 5** shows the geometric structure parameters for a full cell setup with two-layered electrodes. Each of the four electrode layers has three individual parameters that may be changed: the AM volume fraction ϵ , the particle radius R , and the layer thickness d . Consequently, derived parameters like the electrolyte volume fraction, the geometrical tortuosity, and the electric conductivity may differ in each layer. The governing equations for solid diffusion, solid potential, electrolyte potential, and electrolyte diffusion are extended to the additional layer within each electrode. For a consistent application of the finite volume method, the spatial dependence of electrode parameters like layer thickness, porosity, or particle size and the corresponding spatial dependence of their derived parameters like the electrolyte volume fraction or solid conductivity must be considered for the electrode

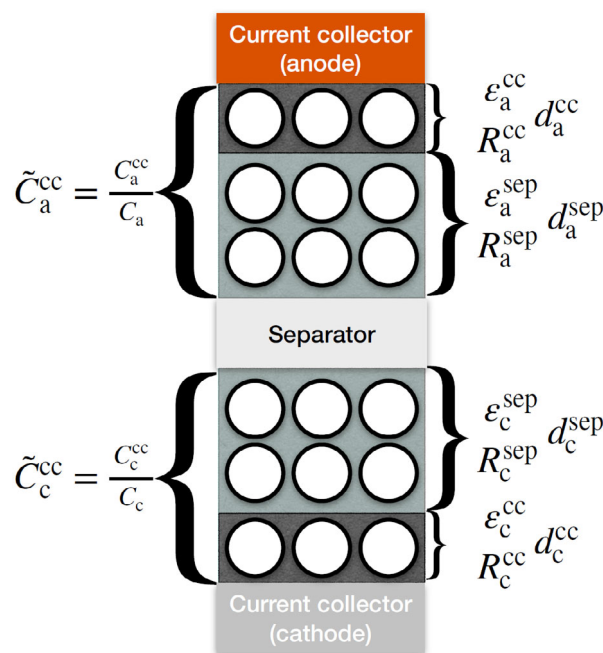


Figure 5. Lithium-ion battery cell with two layers of different properties in each electrode. For parameter variations, three structure parameters can be changed per layer: the AM volume fraction ϵ , the particle radius R , and the layer thickness d . The parameter C^{cc} describes the ratio between the theoretical capacity in the layer adjacent to the current collector C^{cc} (dark grey layer) and the total theoretical capacity C (dark + light grey layer) and enables a more intuitive understanding of the capacity contribution of the two layers within each electrode.

meshing. Taleghani et al. provide a detailed summary of applicable boundary conditions in a P2D model for a two-layered versus a single-layered electrode.^[50] For all simulations in this work, the electrode- and particle-level discretization of each electrode layer is fixed to 5 and 4, respectively. Simulations of configurations that do not converge and exceed 15 min simulation time compared with a typical simulation time of less than 1 min are terminated and the results discarded. All simulations were conducted with MATLAB version 2019a or newer, using the solver ode15s.

The parameter set is largely adopted from the battery model with extended structure–parameter relations in the study by Laue et al. and shown in **Table A2** in the Appendix.^[27] To enable a realistic representation of transport properties as a function of electrode structure, Laue's effective polynomials from 3D microstructure simulations for the active surface area, the effective ionic conductivity, and the electric conductivity of the cathode are adopted as well. Equally, the volume ratio between AM and CBD for the cathode of 4.4/1 is adopted. It is defined for the anode at a higher value of 10/1 due to the good conductivity of graphite. In general, the 3D microstructure simulations were conducted for a particle size of 5.5 μm . However, an adjustment of the polynomials based on additional microstructure simulations for the later-defined particle size variations is out of the scope of this work. Nonetheless, a quantitative design recommendation for an experimental study would require this adjustment as well as a corresponding validation with experimental data. The utilized polynomials and other complementary model equations are shown in **Table A3** in the Appendix.

In Laue's work, the empirical polynomials were derived for the cathode side only. Considering the relatively high electric conductivity of the anode AM, a polynomial is not deemed necessary for this anode parameter. Its effective electric conductivity is simply calculated from the AM volume fraction. For the calculation of the effective ionic conductivity and diffusivity within the electrolyte phase of the anode, its tortuosity is described via the commonly used Bruggeman equation along with a Bruggeman exponent β of 1.5, which describes ideal spheres.^[95] The active surface area is commonly calculated based on the assumption of ideal spherical particles with a linear dependence on the AM volume fraction. However, for very high AM volume fractions, this approximation is not valid anymore as the active surface area cannot be highest in a material without any free volume. To circumvent this unrealistic behavior and despite potentially different particle shapes, the effective polynomial for the cathode active surface area is also used for the anode side.

The concentration-dependent ionic conductivity and diffusivity of the 1 M LiPF₆ EC:EMC 3:7 (w:w) electrolyte system are described by empirical polynomials that were fitted to experimental data by Landesfeind et al.^[96] The anode and cathode open-circuit potential are described with empirical expressions as a function of state of charge.^[27]

For the second parameter study, a two-layered cathode half cell is investigated. In contrast to the full cell model, the graphite-based anode is replaced with a lithium metal counter electrode that is modeled as a boundary condition, i.e., it provides the amount of lithium ions that corresponds to the externally applied current density. This ensures an interaction-free evaluation of the cathode design for lithium intercalation but inherently also

limits its value for the direct estimation of the performance of such an optimized cathode in a full cell setup. Apart from different parameter variations, the same parameters and equations are used for the cathode in the full and half cell study.

3.2. Case Study Definition

3.2.1. Full Cell Parameter Study

The first step toward electrode design optimization is the definition of an optimization objective. For this study, four application scenarios are defined, i.e., discharge and charge at 0.1C and 1C. The high and low C-rate will enable an assessment of transport limitations as a function of applied load. To enable a direct comparison between discharge and charge performance, the voltage-independent capacity is used as the evaluation metric. For a mathematical design optimization, it would be required to choose between areal, volumetric, and gravimetric capacity or incorporate multiple objectives into a then more complex optimization process. Such a kind of trade-off is obsolete for a parameter study with predefined parameter variations. By this approach, the simulation data can simply be analyzed with respect to areal, volumetric, and gravimetric capacities at all investigated C-rates. For all studies in this work, the theoretical capacity, i.e., the mass loading of each electrode, is fixed as a boundary condition so that the gravimetric and areal capacity are qualitatively equivalent. To enable a more intuitive comparison with the volumetric capacity, the areal capacity is chosen instead of the gravimetric capacity. Here, the volumetric capacity inherently includes a trade-off between electrode volume and potentially reduced mass transport losses in porous electrodes compared with the volume-independent areal capacity. In summary, the chosen optimization targets for the parameter studies in this work are the areal and volumetric discharge and charge capacities at C-rates of 0.1C and 1C with typical cutoff cell voltages at 2.9 and 4.2 V. The diversity of these application scenarios along with a detailed analysis of both areal and volumetric performance metrics will enable an in-depth understanding of the interrelation between structure recommendations and their application-specific performance.

For the calculation of the volumetric capacity, double-sided coated electrodes are assumed. As a result, the full thickness of the separator (20 μm) but only half the cathode (20/2 μm) and half the anode (10/2 μm) current collector thickness must be considered. The theoretical capacities of anode and cathode are balanced 1.1/1 such that the anode capacity is 10% larger than the cathode capacity. This is a common design choice to mitigate lithium plating.^[6,8] As this is an electrode design study focusing on capacity improvements, we do not consider sophisticated charging protocols, e.g., to prevent lithium plating.

The parameter variations for the full cell parameter screening are defined based on the schematic cell structure in Figure 5. Two-layered electrodes are investigated to gain a better understanding of limiting processes within thick electrodes by allowing for different structural properties in each layer. Importantly, a fine-grained evaluation of the whole parameter space is infeasible due to the resulting combinatorial explosion with 12 examined geometric structure parameters: these are for each of the four layers the layer thickness, the AM volume fraction, and the particle radius. For the full cell and also half cell study study, the

theoretical cathode capacity is fixed to 5 mAh cm^{-2} , which is roughly in between an ultra-high and a state-of-the-art mass loading (see Figure 1a). This choice ensures diverse performance characteristics with poor performance at 1C for overly dense electrodes and reasonable performance for well-designed electrodes. The theoretical capacity is calculated based on the maximum lithium concentration within the AM of anode and cathode.

The capacity fixation already reduces the degrees of freedom to ten design parameters. However, this still results in $3^{10} = 59049$ full cell configurations for just three variations per design parameter. With the focus on the investigation of general electrode design principles for both charge and discharge, we therefore reduce the number of simulations by investigating just two particle size variations for all four electrode layers. The choice of the particle radii of 3 and $9 \mu\text{m}$ represents typical particle sizes.^[27,97]

A variation of the cathode AM volume fraction has a pronounced effect on both the mass transport in the electrolyte phase that deteriorates with decreasing porosity and the electric conductivity of the solid phase that is highly sensitive around the percolation threshold. For this reason, three variations are defined, leading to effective conductivities that differ by one order of magnitude each. This introduces cathodes with poor, intermediate, and good effective electric conductivity into the parameter study. On the anode side, ohmic losses are less of an issue due to the high electric conductivity of the graphite AM. Nonetheless, mass transport in the electrolyte phase still deteriorates nonlinear with decreasing porosity. For this reason, the same AM volume fractions as for the cathode are chosen for the anode.

For the last two degrees of freedom, we introduce for both anode and cathode a dimensionless parameter \tilde{C}^{cc} , i.e., the ratio between the theoretical capacity in the layer adjacent to the current collector and the total theoretical capacity of the electrode. This enables a better understanding of the capacity that is provided by each layer within a two-layered electrode. Two variations are defined for \tilde{C}^{cc} with either 25% or 75% of the electrode capacity provided by the layer adjacent to the anode and cathode current collector, respectively. In the end, this results in 5184 cell configurations for the full cell parameter screening with four simulations each to cover charge and discharge at 0.1C and 1C. **Table 1** shows the chosen parameter values for the model-based full cell design screening.

Table 1. Definition of the parameter variations for the rapid full cell electrode design screening.

Parameters	Low value	Medium value	High value
ϵ_a^{cc} [-]	0.45	0.55	0.65
ϵ_a^{sep} [-]	0.45	0.55	0.65
ϵ_c^{sep} [-]	0.45	0.55	0.65
ϵ_c^{cc} [-]	0.45	0.55	0.65
R_s^{cc} [μm]	3	–	9
R_s^{sep} [μm]	3	–	9
R_c^{sep} [μm]	3	–	9
R_c^{cc} [μm]	3	–	9
\tilde{C}_a^{cc} [%]	25	–	75
\tilde{C}_c^{cc} [%]	25	–	75

To evaluate the effect that the prevention of lithium plating during 1C charge has on optimal electrode design, the full cell design screening is repeated with a slight modification. In this case, the charge operation can additionally be terminated when the local anode potential falls below 0 V versus Li/Li^+ , which would trigger lithium plating.

Finally, a suitable benchmark system must be defined for the four different application scenarios. For this purpose, the performance of the best structured cell configuration for a specific application is compared with the best single-layered cell configuration within the predefined parameter space. This resembles an experimental parameter screening, which may not have access to an optimized benchmark system and must resort to one of the investigated cell configurations for comparison.

Overall, the first case study provides with its coarse-grained parameter screening a rough overview of the parameter space. However, with only two or three values per design parameter, the study does not provide an insight into how sensitive the result is to small or medium changes in these parameter. Such a more detailed analysis can be done by evaluating significantly more values for each parameter, albeit, to keep the model-based study computationally feasible, the number of parameters or the complexity of the model in such a study has to be significantly reduced. This is subject of the second case study that is described in the following section.

3.2.2. Half Cell Parameter Study

To enable a closer look at the design parameter space for a two-layered electrode, we limit this case study to a cathode half cell. Here, the cathode is deemed more insightful compared with the anode due to the poor electric conductivity of the cathode AM that depends strongly on the percolation network formed by the CBD. To allow for an intuitive graphical visualization, typically only two parameters are varied.^[38,42,89] With a fixed theoretical capacity of 5 mAh cm^{-2} , the design parameter space contains five degrees of freedom and will be further reduced to two design parameters. The full cell parameter screening will reveal a low sensitivity of cell performance to cathode particle size for the utilized parameter set. Consequently, the AM particle radius is fixed to $3 \mu\text{m}$. Further, we choose a fixed average AM volume fraction of 55%, which is the average value used for the parameter variations in the full cell parameter screening. With this fixation of both theoretical capacity and average AM volume fraction, the combined coating thickness of both cathode layers is fixed to $133.4 \mu\text{m}$.

The two remaining degrees of freedom are the AM volume fraction in the layer at the separator along with the thickness of this layer. In other words, a decrease in the AM volume fraction in one layer must be compensated by an increase in the AM volume fraction in the other layer. The cathode AM volume fraction at the separator is varied between the minimum (45%) and maximum (65%) values that are used in the full cell study. The thickness of the layer at the separator is varied between 10% and 90% of the fixed total cathode coating thickness. Both parameters are varied in steps of 0.5 percentage points. Parameter configurations that would require an AM volume fraction beyond the investigated minimum and maximum value are discarded and

assigned a capacity of zero. As a result of the fixed coating thickness and theoretical capacity, a single-layered benchmark electrode is already defined and may be regarded as an optimized benchmark. This enables a critical assessment of the benchmark definition in the full cell study that uses the best homogeneous electrodes from the parameter screening instead of a predefined optimized system.

As discussed earlier, only the intercalation into the cathode, i.e., the full cell discharge process, can be studied consistently with the lithium metal counter electrode implemented as a boundary condition. For the deintercalation, i.e., the charge direction in a full cell setup, the electrolyte concentration could drop below zero as a result of the concentration-independent implementation of the counter electrode. Furthermore, considering the fixation of both theoretical capacity and coating thickness, cell performance at 0.1C can be expected to be almost independent of the electrode structure. For this reason, only intercalation at 1C is investigated.

4. Results

First, the results from the full cell parameter screening are shown and discussed with respect to 1) general electrode design guidelines for optimal performance during discharge and charge and 2) the expected benefit from two-layered electrodes when compared with the best-in-class single-layered cell configurations in the parameter study. Subsequently, the relevance of lithium plating during charge at 1C for cell design is analyzed. In the second part, the benefit from electrode structuring is evaluated from the perspective of the fine-grained cathode half cell parameter study. Here, a special focus is on the importance of the parameter space surrounding an electrode design point for robust electrode production. Finally, the results from the full and half cell study are compared.

4.1. Full Cell Parameter Study

The discussion of the full cell parameter screening results is broken down into four parts. First, a comprehensive overview of the more than 5000 simulated cell configurations is provided. Second, the best performing cells with respect to charge and discharge at 1C and 0.1C are identified and analyzed in more detail. Here, also the difference between areal and volumetric capacity is discussed regarding its effect on favored cell designs for best performance. The third section discusses the unexpected benefit of larger particles at the separator. Finally, it is investigated in how far lithium plating may occur during 1C charge in the best cell configurations that are tailored for 1C discharge and charge, respectively.

4.1.1. Parameter Screening Overview

Figure 6 shows the charge and discharge performance of all simulated full cell configurations at C-rates of 0.1C (grey and green colors) and 1C (black and red colors). The parameter variations are sorted by their volumetric discharge capacity at 1C. This kind of visualization reveals three fundamental aspects. First, a large number of simulated cell configurations leads to cells with a poor

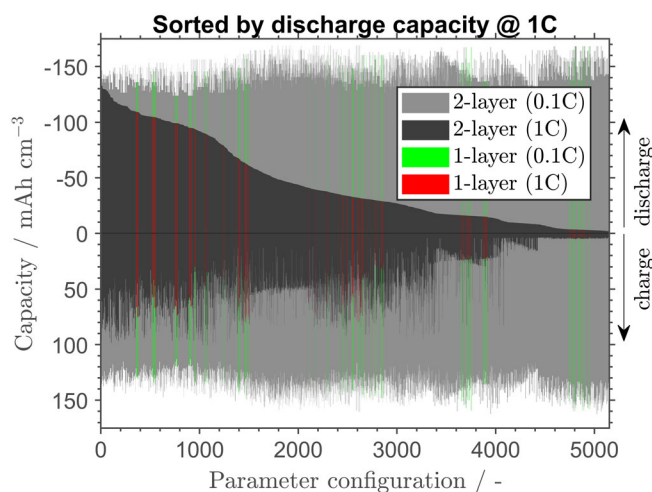


Figure 6. Performance comparison of all investigated parameter variations for cells with two-layered electrodes, sorted in descending order by their volumetric discharge capacity at 1C. Discharge is shown with negative values, charge with positive values. Full cell configurations that lead to single-layered electrodes for both anode and cathode are highlighted.

discharge and charge performance at 1C while delivering a similar capacity at 0.1C due to the fixation of the theoretical capacity. Second, the discharge capacity at 1C is not directly related to the charge capacity, i.e., a cell with a lower discharge capacity may feature a higher charge capacity and vice versa. This holds true for both single-layered and two-layered cell configurations. This finding underlines the necessity to consider both discharge and charge performance for cell design optimization. Inference from discharge to charge performance is not advised. Third, apart from cells with best-in-class performance for a specific application, there are also cell configurations among the more-than-5000 samples, which show almost similar performance for charge and discharge at 1C. For an overview of possible performance characteristics, it is thus worthwhile to conduct a coarse-grained parameter screening as presented here.

4.1.2. Implications of Performance Metrics for Cell Design

Figure 7 shows the best cell configurations for the four different operating modes, i.e., discharge and charge at 0.1C as well as discharge and charge at 1C. The best single-layered cell configuration for each of these applications is shown for comparison with thin, colored bars. In the following paragraphs, the performance characteristics and corresponding electrode structures of the best-in-class cell configurations for the four different operating modes are discussed, starting with the areal capacity in Figure 7a and ending with the volumetric capacity in Figure 7b.

As a first observation, the best cell configurations for charge and discharge at 1C feature almost the same areal capacities at 0.1C as the cells that are explicitly tailored for 0.1C applications. This would suggest that cells can be optimized directly for 1C discharge or charge without any worries about their performance at 0.1C. There is also no significant benefit of two-layered over single-layered cells if both are tailored for charge or discharge at 0.1C as the cell voltage is only slightly affected by transport

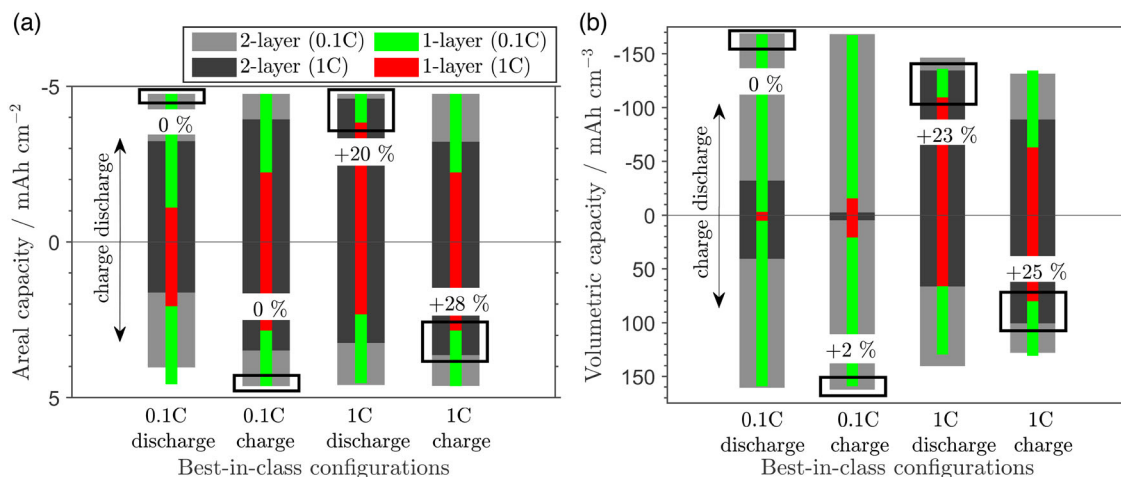


Figure 7. A comparison of performance of best-in-class cell configurations with single-layered (thin bars) and two-layered electrodes (wide bars) for discharge at 0.1C, charge at 0.1C, discharge at 1C, and charge at 1C. The best-in-class cell configurations from the full cell study are selected both a) for the areal capacity and b) for the volumetric capacity. The performance focus of the best-in-class configurations is highlighted by black boxes. Percentage performance gains indicate the increase in capacity when comparing two-layered versus single-layered electrodes for each operating mode. The corresponding structure parameters for the two-layered and single-layered cell configurations for the areal capacity are shown in Table 2 and 3 and for the volumetric capacity in Table 4 and 5.

processes at such low C-rates. In contrast, the areal capacities of the best two-layered cells for discharge and charge at 1C are notably higher than the best single-layered cell configurations with an improvement of 20% and 28%, respectively.

It should be noted that the observed performance improvement of up to 28% with structured electrodes may originate from the coarse parameter screening, which underlies this study. A finer grid for the parameter screening, i.e., a simple brute-force optimization, would most probably enable a better trade-off between transport losses in the electrolyte and solid phase. For most practical design problems, a direct mathematical optimization should be preferred due to a more efficient exploration of the parameter space. Eventually, coarse experimental and model-based parameter studies alike can only reflect the improvement either over an arbitrary benchmark cell or over the best homogeneous cell configuration from the parameter study itself. In contrast, an optimized homogeneous benchmark system would presumably result in a less significant performance benefit from electrode grading. This is highlighted by the earlier discussed model-based study by Dai et al., who investigated a full cell setup with varying cathode porosity over the electrode thickness.^[42] Compared with an optimized homogeneous electrode, they observed only a 3% energy density improvement.

In the following section, the above mentioned performance improvement of graded over single-layered electrodes is discussed with respect to the actual electrode structures. Table 2 and 3 show the specific structure properties of the best two-layered and single-layered cell configurations for highest areal capacity.

For discharge at 1C, the best structured cell uses a cathode that provides 25% of the capacity in a medium porous layer at the current collector (55% AM volume fraction) and 75% of the capacity in a highly porous layer at the separator (45% AM volume fraction). This ensures good electric conductivity near the current collector while facilitating mass transport into the deeper electrode structure by the more porous layer at the separator.

Table 2. Identified parameter values in the full cell parameter study for highest areal capacity for the four different operating modes with two-layered electrodes.

Parameters	Discharge @ 0.1C	Charge @ 0.1C	Discharge @ 1C	Charge @ 1C
ϵ_a^{cc} [-]	0.65	0.45	0.45	0.45
ϵ_a^{sep} [-]	0.55	0.45	0.55	0.45
ϵ_c^{sep} [-]	0.45	0.45	0.45	0.45
ϵ_c^{cc} [-]	0.55	0.65	0.55	0.55
R_a^{cc} [μm]	9	3	3	3
R_a^{sep} [μm]	3	3	3	9
R_c^{sep} [μm]	3	9	3	9
R_c^{cc} [μm]	3	9	3	9
\tilde{C}_a^{cc} [%]	75	25	75	75
\tilde{C}_c^{cc} [%]	75	25	25	75

Table 3. Identified parameter values in the full cell parameter study for highest areal capacity for the four different operating modes with single-layered electrodes.

Parameters	Discharge @ 0.1C	Charge @ 0.1C	Discharge @ 1C	Charge @ 1C
ϵ_a [-]	0.55	0.45	0.55	0.45
ϵ_c [-]	0.45	0.55	0.55	0.55
R_a [μm]	9	3	3	3
R_c [μm]	3	9	3	9

In contrast, the best homogeneous cell configuration cannot make this kind of trade-off. Instead, it uses a cathode with an AM volume fraction of 55%. This leads to an overall deteriorated discharge performance at 1C because of an increased mass

transport resistance that cannot be compensated by the improved electric conductivity. On the anode side, the layer at the current collector provides 75% of the total anode capacity with an AM volume fraction of 45%, whereas the layer adjacent to the separator has an AM volume fraction of 55%. At first sight, this is unexpected. Nonetheless, a thin layer with medium porosity at the separator seems to enable a more homogeneous AM utilization throughout the anode. A similar effect will be discussed later for the anode particle size.

For charge at 1C, mass transport seems to be the most relevant issue on the anode side, favoring the smallest AM volume fraction in both layers. On the cathode side, the AM volume fraction in the layer at the current collector is still 55% and at the separator 45%. However, in contrast to discharge at 1C, the highly porous layer at the separator accounts for only 25% instead of 75% of the total cathode capacity, favoring a higher electric conductivity over a lower transport resistance for charge at 1C. Overall, the performance deviation between the best structured and the best homogeneous cell configurations seems to originate from a better trade-off between sluggish transport in the electrolyte phase of too dense electrodes and low electric conductivity in the solid phase of too porous electrodes.

For applications without volume constraints, the areal capacity seems to be a reasonable evaluation metric that allows cell design optimization to focus on the performance at 1C. However, the volumetric capacity in Figure 7b draws a different picture. Here, it is clearly visible that the cell configurations tailored to 1C applications cannot deliver the same volumetric capacity at 0.1C as the ones explicitly tailored to 0.1C charge and discharge. In comparison with the areal capacity, there is not anymore only one trade-off between charge and discharge performance at 1C, but there is also a trade-off between the performance at 0.1C and 1C.

When comparing the best-in-class cells for discharge and charge at 1C, the difference between the best two-layered and the best single-layered cell configurations is significant with 23% and 25%, respectively. This benefit of electrode structuring is in about the same range as for the areal capacity. The identified best structure parameters for all four operating modes with the volumetric capacity as the performance metric are shown in Table 4 and 5 for the two-layered and single-layered cell configurations, respectively. To account for the higher complexity of the results for the volumetric capacity, the discussion is supplemented by a Sankey diagram in Figure 8, which visualizes the required structure properties for the best-in-class full cell configurations from Figure 7b. Here, the flows link the four different application scenarios on the left side to the required structure parameters for best-in-class volumetric capacity on the right side. Structure properties that are used for both charge and discharge at 1C are highlighted. Due to almost negligible mass transport losses for 0.1C charge and discharge, the recommended structures are mostly dense and feature the highest AM volume fraction. Only for discharge at 0.1C a thin cathode layer at the separator with a medium AM volume fraction of 55% is required. Compared with the performance of the cell configurations for a high areal capacity at 0.1C, these relatively dense structures have a devastating effect on the performance at 1C (see Figure 7b). Again, there is no significant benefit of two-layered over single-layered cell configurations for discharge at 0.1C and an almost negligible improvement of 2% for charge at 0.1C.

Table 4. Identified parameter values in the full cell parameter study for highest volumetric capacity for the four different operating modes with two-layered electrodes. The best cell configurations for charge and discharge at 1C are the same for both the initial parameter screening, which did not control for lithium plating, and the subsequent parameter screening, which terminated charging below 0V versus Li/Li⁺ to prevent lithium plating.

Parameters	Discharge @ 0.1C	Charge @ 0.1C	Discharge @ 1C	Charge @ 1C
ϵ_a^{cc} [-]	0.65	0.65	0.65	0.45
ϵ_a^{sep} [-]	0.65	0.65	0.55	0.45
ϵ_c^{sep} [-]	0.55	0.65	0.45	0.45
ϵ_c^{cc} [-]	0.65	0.65	0.55	0.55
R_a^{cc} [μm]	3	3	3	3
R_a^{sep} [μm]	9	9	9	9
R_c^{sep} [μm]	3	3	3	9
R_c^{cc} [μm]	3	3	3	9
\tilde{C}_a^{cc} [%]	75	25	75	75
\tilde{C}_c^{cc} [%]	75	25	25	75

Table 5. Identified parameter values in the full cell parameter study for highest volumetric capacity for the four different operating modes with single-layered electrodes. The best cell configurations for charge and discharge at 1C are the same for both the initial parameter screening, which did not control for lithium plating, and the subsequent parameter screening, which terminated charging below 0V versus Li/Li⁺ to prevent lithium plating.

Parameters	Discharge @ 0.1C	Charge @ 0.1C	Discharge @ 1C	Charge @ 1C
ϵ_a [-]	0.65	0.65	0.55	0.45
ϵ_c [-]	0.65	0.65	0.45	0.55
R_a [μm]	3	3	9	3
R_c [μm]	3	9	3	9

When looking at the parameter values that are recommended for both charge and discharge at 1C, it seems important that the anode provides most of the capacity (75%) with small particles at the current collector and the remainder of the capacity (25%) with large particles at the separator. At first sight, this seems counterintuitive and will be addressed in the following section. On the cathode side, the lowest and medium AM volume fraction are favored at the separator and current collector, respectively. This structure provides decent electric conductivity toward the current collector while maintaining sufficiently fast lithium transport through the porous layer at the separator into the deeper electrode structure. The highest cathode AM volume fraction is only relevant with a focus on 0.1C applications. This trend toward denser cathodes for lower C-rates is in good agreement with the experimental study by Schmidt et al. and highlights the challenge of proper cathode design.^[24] On the one hand, a high porosity is required to facilitate mass transport. On the other hand, a higher densification, i.e., a smaller porosity, is required for adequate electric conductivity. Without an accurate consideration of these two relations on the modeling side, e.g., with approximations from microstructure simulations like those used

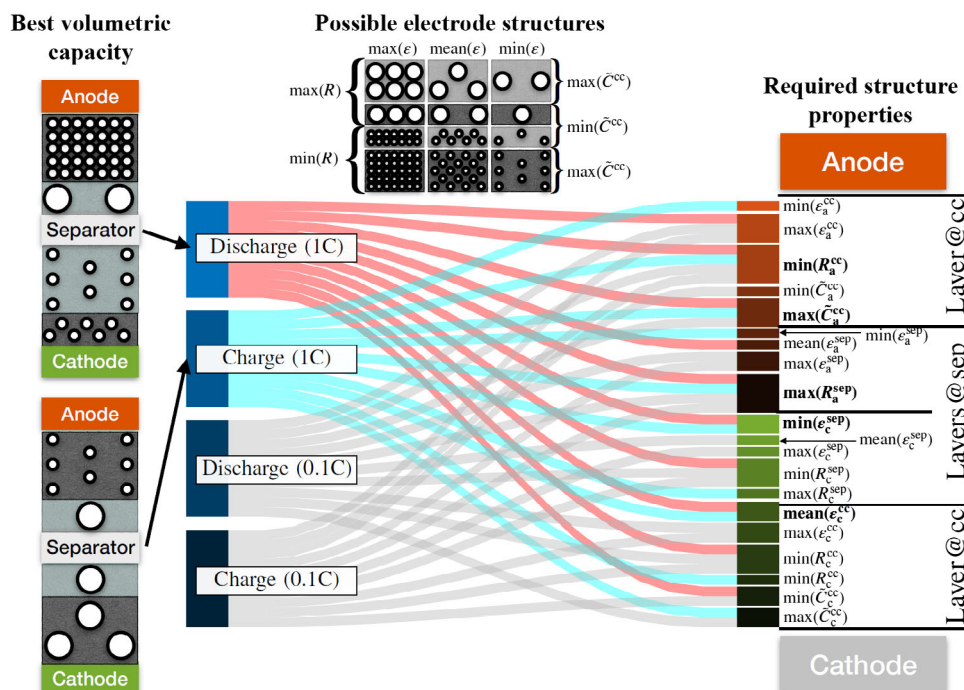


Figure 8. Sankey diagram with application scenarios on the left side and required structure properties on the right side. The desired application focus, i.e., discharge or charge at 0.1C or 1C, is translated through the flows into the individually required structure properties for best volumetric capacity. Structure properties that are required for both charge and discharge at 1C are printed bold to facilitate the comparison with the 0.1C application scenarios. The best cell structures for discharge (red flows) and charge (turquoise flows) at 1C are schematically shown on the left side. A legend for the relation between varied parameters and schematic electrode structures is shown at the top. The Sankey diagram was created with the MATLAB code from Wang.^[103]

in this work, a model-based design optimization could leave the validity range of the underlying model early on, potentially providing poor design recommendations.

4.1.3. The Counterintuitive Effect of Particle Size

A more detailed analysis of the anode structure for charge at 1C reveals an unexpected benefit of large anode particles in a thin layer at the separator (25% capacity) and small particles at the current collector (75% capacity). This design resembles the continuous particle radius profile in the model-based study by Golmon et al. (see Figure 3).^[35] However, they did not investigate charging. Although small particles may generally be expected to provide better performance due to a larger surface area with enhanced reaction kinetics and a reduced solid diffusion length, the results indicate that the larger particles at the separator compared with smaller particles actually improve the volumetric charge capacity by roughly 11%. For discharge, the design principle is the same: small particles at the current collector to minimize the overpotential and large particles at the separator to achieve a more homogeneous AM utilization throughout the electrode. However, the 1% benefit compared with small particles is insignificant. On the cathode side, the difference in the 1C charge capacity with small particles compared with large particles is even less significant with only 0.01%. For the used parameter set, the cathode particle size seems insensitive due to very fast reaction kinetics and fast solid diffusion.

To enable a better understanding of the sensitivity of the particle size, the five best-in-class cell configurations for discharge at 1C (Table A4) and charge at 1C (Table A5) are shown in the Appendix along with their corresponding volumetric capacities for all four modes of operation. The fact that the particle size on the anode side always remains the same, whereas the particle size in the two cathode layers changes seemingly randomly, underlines the low sensitivity of the cathode AM particle size and the significance of larger anode particles at the separator. This points at the fundamental necessity to focus on sensitive parameters during an optimization. Without a prior sensitivity analysis, an optimization could lead to structure recommendations without any substantial benefit.

4.1.4. Cell Design for Lithium-Plating-Free Charging

Apart from the pronounced benefit of electrode structuring for 1C applications in this case study, the results strongly suggest that the best-in-class charge and the best-in-class discharge characteristic at 1C cannot be achieved with the same electrode structure. The performance improvement of a cell tailored to charge at 1C compared with the one tailored to discharge at 1C is about 51%. Vice versa, the improvement is coincidentally also 51%. This underlines that a proper optimization has to find a trade-off between cell design for charge and discharge requirements.

It should be noted that, for the sake of simplicity, we presented a case study with constant current for charge and discharge without any safety- or aging-related considerations. However, safety

critical effects like lithium plating can easily be studied with the used battery model.^[6] **Figure 9** takes this point up and compares the 1C charge performance of the best-in-class cell for 1C discharge with the best-in-class cell for 1C charge in the context of lithium plating. For the two bars on the left side, charging was terminated upon reaching the upper cutoff cell voltage of 4.2 V, equivalent to Figure 7. For the two bars on the right side, the charge simulations could additionally be terminated upon reaching a local anode potential below 0 V versus Li/Li⁺, which would result in lithium plating. Interestingly, the structure of the best cells without the possibility of lithium plating is the same as for the already discussed parameter screening, which did not control for lithium plating. Hence, the structure parameters of the two- and single-layered electrodes are the same as in Table 4 and 5. Due to a comparable interpretation for both homogeneous and structured cell configurations, the following discussion will focus on the better performing structured cells.

When comparing the performance characteristic of the two best-in-class cells that show no lithium plating, the cell tailored to discharge at 1C of course still provides the same 51% benefit for discharge at 1C over the one tailored for charge at 1C. However, with the described lithium-plating prevention measure in place, its charge capability at 1C is significantly deteriorated. For comparison, the cell tailored for 1C charge has a 160% higher charge capacity than the one designed for 1C discharge, which basically fails to achieve a reasonable charge performance. This

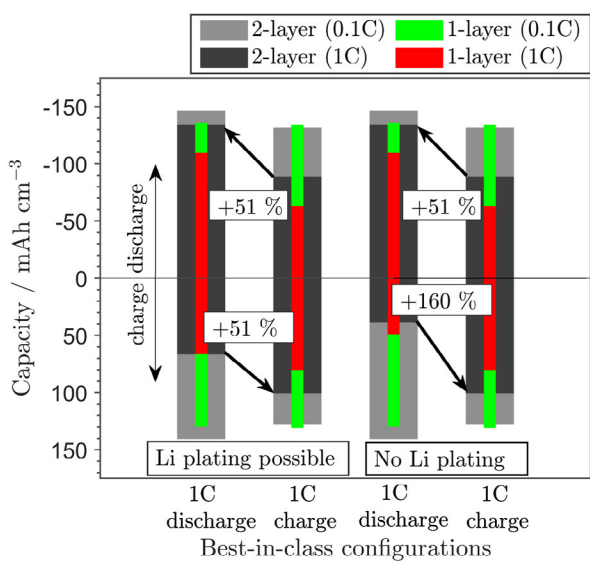


Figure 9. A comparison of volumetric capacity of best-in-class electrode configurations for single-layered (thin bars) and two-layered electrodes (wide bars) selected from the full cell study for discharge and charge at 1C. For the two bars on the left side, charge simulations were terminated upon reaching 4.2 V cell voltage. For the two bars on the right side, charge simulations were terminated upon reaching 4.2 V or upon reaching a local anode potential below 0 V versus Li/Li⁺. Percentage performance gains indicate the increase in capacity when comparing the structured cells tailored to charge with the one tailored to discharge at 1C and vice versa. The best two- and single-layered cell configurations for the no-plating cases are identical to the configurations for cases where plating is possible (see Table 4 and 5).

finding further highlights the absolute necessity to tailor a cell not only to the discharge requirements of a given application but also to the required charge performance. Future studies may consider incorporating additional aspects besides lithium plating into cell design optimization. For instance, Golmon et al. already incorporated an upper limit for the mechanical AM particle stress into the design optimization.^[51] This may be further extended to long-term growth of the solid electrolyte interphase,^[98,99] as well as mechanical degradation of the AM.^[100]

Overall, the presented coarse-grained multi-parameter screening, i.e., a simple brute-force optimization, should be seen as a valuable tool to identify basic trends that may be used as a basis for further optimization. Due to the chosen large design parameter space with ten degrees of freedom, the parameter screening is likely too coarse grained to identify the global optimum. Such an analysis requires a higher resolution of the parameter space as presented in the following half cell parameter study. Considering that even more than 5000 simulations cannot provide a comprehensive understanding of the whole design parameter space, a sufficiently broad experimental study seems infeasible at the moment without an automated high-throughput production and testing of diverse electrode variations. However, the conducted model-based brute-force screening should also only be used if basic trends in the parameter space are relevant. Otherwise, a model-based design optimization would also benefit from a more efficient exploration and exploitation of the available design parameter space. Eventually, even with DOE, experimental studies will have to focus on the investigation of design highlights. These may be derived from experimental observations and experience or model-based predictions. Independent of the selected experiments, we recommend to consider both discharge and charge directions in practically relevant performance ranges to provide a more holistic understanding and a faster adoption of the investigated process or electrode design advancements.

4.2. Half Cell Parameter Study

In this section, the results from the fine-grained cathode half cell study are discussed. The significantly reduced design parameter space with only two degrees of freedom allows for a higher resolution compared with the full cell design screening. This does not only enable a good approximation of the optimal electrode structure, but it also allows for a detailed assessment of the local interrelation between design parameters and usable capacity in proximity of the optimal electrode structure. As already discussed, the full cell parameter study was not designed to provide this level of detail. This contrast between the coarse full cell screening and the highly discretized half cell study will help to put the roughly 20% performance benefit of two-layered electrodes from the full cell study into perspective.

Due to the definition of a constant particle radius, theoretical capacity, and average AM volume fraction, the cathode structure can be defined by two parameters: the thickness of the layer at the separator and the AM volume fraction in this layer. This means that an AM volume fraction at the separator below average directly results in a higher AM volume fraction at the current collector and vice versa. Due to the constant coating thickness, the areal and volumetric capacity are directly proportional to each other.

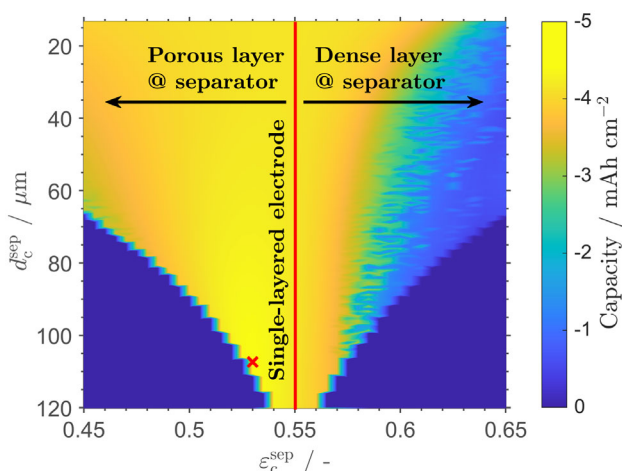


Figure 10. Parameter study for a two-layered cathode with a fixed theoretical capacity of 5 mAh cm^{-2} and a fixed average AM volume fraction of 55%, corresponding to a coating thickness of $133.4 \mu\text{m}$. The red line represents single-layered electrode configurations. The color scale describes the areal capacity for intercalation, i.e., full cell discharge, at 1C. The optimum is highlighted with a red cross. Due to the fixed coating thickness and theoretical capacity, the volumetric capacity is directly proportional to the areal capacity.

For this reason, **Figure 10** shows the cathode parameter study with the more intuitive areal capacity as a performance measure.

The results indicate that the best capacity is obtained with a slightly more porous layer at the separator compared with the layer at the current collector. This general structuring recommendation is in good agreement with the prior full cell study. It also resembles findings from other studies in the field for both half cell and full cell studies.^[35,38,40,42] For the study conducted in this work, the advantage of the best two-layered cathode is 5.9% compared with the single-layered benchmark.

Of higher practical relevance for electrode design than the estimated performance improvement could be the large capacity plateau located around the single-layered electrode configuration. This suggests that the AM distribution and thus the porosity distribution within the electrode may be varied over a wide parameter range without significantly altering the performance. For electrode production, such a large parameter field with comparable performance characteristics is likely to facilitate the adaptation of already established production processes. However, it should be noted that this capacity plateau may look different or be nonexistent at all when looking at a full cell instead of a half cell configuration or when changing the fixed parameters, e.g., the theoretical capacity, the average AM volume fraction, or the particle size. For a reliable design recommendation, this study would have to be repeated for additionally relevant parameters and should ideally be extended to a full cell setup.

From a slightly different perspective, a large capacity plateau is also favorable for the production of common single-layered electrodes. For a design point in the center of such a plateau, small production variations could be expected to have a small effect on the final electrode performance. However, for large production tolerances or a disadvantageous electrode design selection, the

capacity can deteriorate significantly. Considering the homogeneous electrode as the baseline, the center of mass of the higher discharge capacities is on the side of the electrodes with the more porous layers at the separator. Importantly, the capacity also does not decline as fast for a more porous layer as for a denser layer at the separator. This knowledge on the parameter space surrounding a chosen electrode design can help minimize the detrimental effect of production tolerances on cell performance. The earlier discussed simulation study by Schmidt et al. highlights this aspect as it investigated the effect of production tolerances on the volumetric energy density.^[89] The experimental work by Bockholt et al. further pointed at the intricate interaction of consecutive process steps.^[101] To enable a more sustainable and robust electrode production, future studies on electrode design should consider the utilization of robust optimization approaches to enable a reasonable trade-off between optimal performance and minimal production-related electrode performance variance.

4.3. Comparison of Half and Full Cell Study

When comparing the full cell and half cell study in this work, the estimated benefit from electrode structuring is greatly reduced from roughly 20% to 6%. This highlights the inherent difficulty to compare 1) studies with a realistic (full cell study) versus a nonlimiting counter electrode (half cell study), 2) studies with a similar benchmark, i.e., single-layered electrodes, but with variable versus fixed electrode thickness, and 3) studies with a substantially different resolution of the parameter space. Here, the latter aspect is especially important as the benchmark system in both studies is defined as the best single-layered electrode configuration within the parameter space. The coarse full cell screening cannot ensure the approximation of the global optimum for the single-layered benchmark cell. The same holds true for the best two-layered cell configurations. Ultimately, the coarse full cell parameter screening is a computationally expensive brute-force optimization that should be seen primarily as a tool to identify promising trends within a parameter space. It does not allow for a universal evaluation of the concept of multilayered electrodes if the single-layered benchmark system is not truly optimized. The half cell study has a well-defined single-layered benchmark electrode and indicates that electrode structuring is of minor importance in the defined case study. Nonetheless, it also does not allow for a universal assessment of the concept of multilayered electrodes due to the focus on only a small fraction of the theoretically available design parameter space.

An unbiased estimation of the benefit of the concept of multilayered electrodes for a well-defined optimization objective may be possible with both an optimized single-layered benchmark system and an optimized multilayered electrode. However, the result would still depend on the chosen design parameters, the parameter set, the optimization objective, and the benchmark system. In the end, multilayered electrodes are just one concept within the electrode design toolbox. Its universal assessment would contradict the diversity of its possible application scenarios. As worked out in the first part of the article, this is the general curse of optimization. However, with a well-motivated choice of

values and assumptions, trends and conclusions can be made, which hold in the range of interest.

5. Conclusion and Perspectives

Thick electrodes with a high areal capacity come with the promise of a higher energy density and reduced production costs. However, the increased ratio between active and passive material in cells with thick electrodes also elongates diffusion pathways, which can result in major mass transport limitations at elevated C-rates. The literature overview in the first part of this work revealed a great variety of electrode structuring concepts that can help to mitigate this effect significantly. For the analysis and optimization of these electrode structures, a wide range of physicochemical models is available with different levels of microstructure details. To facilitate the adoption and utilization of published electrode design studies, researchers are encouraged to report performance characteristics that go beyond the actual optimization objective and that cover areal and volumetric metrics as well as charge and discharge performance. This context can help to mitigate the inherent difficulty to select the best suitable electrode design from published research with its underlying variety of research questions and optimization objectives.

The model-based full cell parameter study in this work provides a first systematic analysis of two-layered electrodes for both discharge and charge at 0.1C and 1C. As expected, the difference between cell designs for charge and discharge as well as the advantage of two- over single-layered electrodes is almost negligible at 0.1C due to generally small voltage losses. In contrast, the 1C charge performance of a cell tailored for discharge at 1C was found to differ by 51% from a cell tailored for charge at 1C and, coincidentally, also 51% vice versa. If the charge process is terminated upon safety critical lithium plating, the performance difference for charge at 1C between a cell designed for 1C charge compared with a cell designed for 1C discharge increases to 160%. This divergence of performance characteristics underlines the importance to analyze and report both discharge and charge performance for practically relevant C-rates as part of any electrode design study, whether experimental or model-based. It further highlights that there is not the one universal electrode

design for all application scenarios, pointing at the necessity of a comprehensive optimization problem definition.

The cathode half cell parameter study was conducted with only two design parameters and a high resolution to allow for a detailed understanding of the interrelation between cell performance and electrode structure. The roughly 20% capacity improvement at 1C over the best homogeneous electrode in the full cell study compares to a 6% improvement in the half cell study. Thus, the estimated benefit of multilayered electrodes obviously depends on the screening granularity, the benchmark system, and the optimization setup. Furthermore, the half cell study revealed a significant capacity plateau for cathodes that deviate in porosity only slightly from a homogeneous electrode with a steep capacity decline especially for a denser layer at the separator. Considering production tolerances, the parameter space surrounding an electrode design point should be considered during electrode design to ensure a robust electrode quality, either by a retrospective correlation of experimental production and electrochemical test data, by a stochastic model-based study, or directly within a model-based robust optimization.

From an experimental perspective, the conducted model-based parameter screenings in this work with thousands of simulations raise the question if expensive and limited production capacities are well invested in mere screening or if these resources are better utilized in combination with battery models. In the end, a battery model can provide a design recommendation, but it can hardly be validated without experiments. In turn, an experimental study may find a better cell configuration compared with a specific benchmark, but it cannot reasonably investigate the whole parameter space in the quest for an optimal electrode design. Physicochemical battery models can aid the experimental electrode design optimization 1) by evaluating the expected benefit from different structuring concepts compared with an optimized and unbiased benchmark system, 2) by recommending electrode designs for different application requirements, and 3) by enabling a knowledge-based rather than a retrospective assessment of the effect of production tolerances on the final cell performance.

Appendix

Table A1. Basic equations of the utilized P2D model.^[47,94] L_{cell} denotes the full cell thickness. δ_- and δ_+ describe thickness of anode and cathode, respectively.

Variable	Partial differential equation	Boundary condition
c_s	$\varphi_s(r) = -D_s \frac{\partial c_s(r)}{\partial r}$ $\frac{\partial c_s(r)}{\partial t} = \frac{1}{r^2} \frac{\partial}{\partial r} \left(D_s r^2 \frac{\partial c_s(r)}{\partial r} \right)$	$\varphi_s(0) = 0$ $\varphi_s(R_s) = \frac{j^{\text{Li}}(x)}{a_s F}$
Φ_s	$J_s(x) = -\sigma_{s,\text{eff}} \frac{\partial \Phi_s(x)}{\partial x}$ $\frac{\partial j_s(x)}{\partial x} = -j^{\text{Li}}(x) - j^{\text{DL}}(x)$ $j^{\text{DL}}(x) = a_s C_{\text{DL}} \frac{\partial (\Phi_s(x) - \Phi_e(x))}{\partial t}$	$J_s(0) = \frac{I_{\text{cell}}}{A_{\text{cell}}}$ $J_s(\delta_-) = 0$ $J_s(L_{\text{cell}} - \delta_+) = 0$ $J_s(L_{\text{cell}}) = -\frac{I_{\text{cell}}}{A_{\text{cell}}}$
c_e	$\epsilon_e \frac{\partial c_e(x)}{\partial t} = \frac{\partial}{\partial x} \left(D_{e,\text{eff}} \frac{\partial c_e(x)}{\partial x} \right) + (1 - t_p) \frac{j^{\text{Li}}(x)}{F}$	$\frac{\partial c_e}{\partial x}(0) = 0$ $\frac{\partial c_e}{\partial x}(L_{\text{cell}}) = 0$
Φ_e	$J_e(x) = -\sigma_{e,\text{eff}} \frac{\partial \Phi_e(x)}{\partial x} - \sigma_{\text{De,eff}}(x) \frac{\partial \ln(c_e(x))}{\partial x}$ $\frac{\partial j_e(x)}{\partial x} = j^{\text{Li}}(x) + j^{\text{DL}}(x)$	$\frac{\partial \Phi_e}{\partial x}(0) = 0$ $\frac{\partial \Phi_e}{\partial x}(L_{\text{cell}}) = 0$

Table A2. The parameter set utilized in the model is taken from Laue et al.^[27] Derived variables can be calculated with equations in Table A3 and corresponding parameter variations as defined in Table 1. Fitting parameters relate to the equations in Table A3.

Parameter	Symbol	Anode	Separator	Cathode
Ratio between CBD and AM volume fraction [-]	r_{CBD}	0.1	–	0.2273
CBD volume fraction [-]	ϵ_{CBD}	Table A3 → Table 1	–	Table A3 → Table 1
Electrolyte volume fraction [-]	ϵ_e	Table A3 → Table 1	0.5	Table A3 → Table 1
AM volume fraction [-]	ϵ	Table 1	–	Table 1
Specific surface area [m^{-1}]	a_s	Table A3 → Table 1	–	Table A3 → Table 1
Particle size [μm]	R	Table 1	–	Table 1
Discretization elements in particle [-]	n_p	4	–	4
Discretization elements in cell [-]	n_{cell}	5 & 5	5	5 & 5
Layer thickness [μm]	d	Table A3 → Table 1	20	Table A3 → Table 1
Diffusion coefficient in AM [m^2s^{-1}]	D_s	1.18×10^{-14}	–	4.98×10^{-12}
Diffusion coefficient in electrolyte [m^2s^{-1}]	D_e	Table A3 → Table 1	–	Table A3 → Table 1
Bruggeman coefficient [-]	β	1.5	–	–
Tortuosity [-]	τ	Table A3 → Table 1	1	Table A3 → Table 1
Electrolyte conductivity [Sm^{-1}]	σ_e	Table A3 → Table 1	Table A3 → Table 1	Table A3 → Table 1
AM conductivity [Sm^{-1}]	σ_{AM}	10	–	0.0161
Carbon-binder conductivity [Sm^{-1}]	σ_{CBD}	–	–	760
Charge transfer coefficient [-]	α	0.5	–	0.5
Exchange current density [Am^{-2}]	i_0	0.4935	–	1.2298×10^3
Double-layer capacity [Fm^{-2}]	C_{DL}	0.2	–	0.2
Transference number [-]	t_{\pm}	0.24	0.24	0.24
Reference electrolyte concentration [mol L^{-1}]	$c_{e,\text{ref}}$	1	1	1
Initial electrolyte concentration [mol L^{-1}]	$c_{e,0}$	1	1	1
Theoretical electrode capacity [mAh cm^{-2}]	C_{theo}	5.5^{d}	–	5^{d}
Maximum AM concentration [mol m^{-3}]	$c_{s,\text{max}}$	24 591	–	25 429
Initial concentration for charge [mol m^{-3}]	$c_{s,0,\text{charge}}$	3331	–	25 427
Initial concentration for discharge [mol m^{-3}]	$c_{s,0,\text{discharge}}$	24 564	–	1273.3
Temperature [K]	T	298.15	298.15	298.15
Fitting parameter for $\sigma_{s,\text{eff},c}$ [-]	$\epsilon_{\text{crit,liq}}$	–	–	0.075^{a}
Fitting parameter for $\sigma_{s,\text{eff},c}$ [-]	$\epsilon_{\text{crit,s}}$	–	–	0.2^{a}
Fitting parameter for τ_c [-]	β_1	–	–	2.4049^{a}
Fitting parameter for τ_c [-]	β_2	–	–	Table A3 → Table 1
Fitting parameter for $\sigma_{s,\text{eff},c}$ [-]	β_3	–	–	2^{a}
Fitting parameter for $\sigma_{s,\text{eff},c}$ [-]	β_4	–	–	1.5^{a}
Fitting parameter for $\sigma_{e,\text{eff}}$ [-]	ν_1	–	–	0.9499^{a}
Fitting parameter for $\sigma_{s,\text{eff},c}$ [-]	ν_2	–	–	0.0228^{a}
Fitting parameter for $\sigma_{s,\text{eff},c}$ [-]	ν_3	–	–	0.1^{a}
Fitting parameter for a_s [-]	ν_4	0.9037	–	0.9037
Fitting parameter for a_s [-]	ν_5	1.1270	–	1.1270
Fitting parameter for a_s [-]	ν_6	4.9118	–	4.9118

a: adjusted; d: defined.

Table A3. Complementary equations for the used model. Variables with a tilde are dimensionless.

Equations	Ref.
$j^{\text{Li}}(x) = a_s i_0 \left(\exp\left(\alpha \frac{\eta^{\text{F}}}{RT}\right) - \exp\left((1-\alpha) \frac{\eta^{\text{F}}}{RT}\right) \right)$	[47]
$\eta = \Phi_s(x) - \Phi_e(x) - U_{\text{OCV}}$	[47]
$\varepsilon_{\text{CBD}} = r_{\text{CBD}} \cdot \varepsilon$	[27]
$\varepsilon_e = 1 - \varepsilon - \varepsilon_{\text{CBD}}$	[27]
$\varepsilon_e^* = \frac{1 - \varepsilon - \varepsilon_{\text{CBD}} - \varepsilon_{\text{crit,liq}}}{1 - \varepsilon_{\text{crit,liq}}}, \forall \varepsilon_e \cdot \varepsilon_e > \varepsilon_{\text{crit,liq}}$	[27]
$\varepsilon^* = \frac{\varepsilon - \varepsilon_{\text{crit,s}}}{1 - \varepsilon_{\text{crit,s}}}, \forall \varepsilon \cdot \varepsilon > \varepsilon_{\text{crit,s}}$	[27]
$\varepsilon_{\text{CBD}}^* = \varepsilon_{\text{CBD}} \frac{\varepsilon_{\text{CBD}} + \varepsilon - \varepsilon_{\text{crit,s}}}{1 - \varepsilon_{\text{crit,s}}}, \forall \varepsilon_{\text{CBD}} \cdot \varepsilon_{\text{CBD}} + \varepsilon > \varepsilon_{\text{crit,s}}$	[27]
$d^{\text{CC}} = \frac{C_{\text{theo}}}{F c_{\text{max}}^{\text{e}}} \cdot \tilde{C}^{\text{CC}}$	-
$a_s = \left(1 - \nu_4 \cdot \frac{\varepsilon_{\text{CBD}}^*}{\varepsilon} \right) \cdot \nu_6 \cdot \frac{1 - 4(0.75 - \varepsilon)^2 \cdot \varepsilon_e}{R}$	[27]
$\beta_2 = \varepsilon_{\text{CBD}}^{\beta_1}$	[27]
$\tau_a = \varepsilon_e^{-\beta}$	-
$\tau_c = (\varepsilon_e^*)^{\beta_1 + \beta_2} \cdot \varepsilon_e$	[27]
$\tilde{c}_s = \frac{c_s}{c_{s,\text{max}}}$	-
$\tilde{c}_e = \frac{c_e}{c_{e,0}}$	-
$\sigma_{s,\text{eff},a} = \varepsilon \cdot \sigma_{\text{AM}}$	[27]
$\sigma_{s,\text{eff},c} = \varepsilon \cdot \sigma_{\text{CBD}} \cdot (\varepsilon_{\text{CBD}}^*)^{\beta_3} \cdot \frac{1}{2} \left(1 + \tanh\left(\frac{1}{\nu_2} \varepsilon_{\text{CBD}}^* - \nu_3\right) \right) + \left(\frac{1}{\sigma_{\text{CBD}} \cdot (\varepsilon_{\text{CBD}}^*)^2 + 2\sigma_c \cdot (\varepsilon^*)^{1.5}} + \frac{1}{2\sigma_c \cdot (\varepsilon^*)^{1.5}} \right)^{-1}$	[27]
$\sigma_e = 0.0521 \cdot \left(1 + \left(\frac{T}{K} - 228 \right) \right) \cdot \tilde{c}_e \cdot \frac{(1 - 1.06 \cdot \sqrt{\tilde{c}_e} + 0.353 \cdot (1 - 3.59^{-3} \cdot \exp(\frac{10000}{T})) \cdot \tilde{c}_e)}{1 + \tilde{c}_e^4 \cdot (1.48^{-3} \cdot \exp(\frac{10000}{T}))}$	[96]
$\sigma_{e,\text{eff}} = \frac{\varepsilon_e}{\tau} \cdot \sigma_e$	[27]
$D_e = 1.01 \cdot 10^3 \exp(1.01 \cdot \tilde{c}_e) \cdot \exp\left(\frac{-1.56^2 K}{T}\right) \cdot \exp\left(\frac{-487 K}{T} \cdot \tilde{c}_e\right) \cdot 10^{-10}$	[96]
$D_{e,\text{eff}} = \frac{\varepsilon_e}{\tau} \cdot D_e$	[96]
$U_{\text{OCV},a} = 8.03914 + 5.08225 \cdot \tilde{c}_s - 12.56166 \cdot \sqrt{\tilde{c}_s} + 0.44842 \cdot 10^{-5} \cdot \sqrt{\tilde{c}_s^3} - 0.09620 \cdot \exp(15.0006 \cdot (0.1684 - \tilde{c}_s)) - 0.4599 \cdot \exp(2.3166 \cdot (0.5856 - \tilde{c}_s)) - 0.9575 \cdot \exp(2.4033 \cdot (0.5124 - \tilde{c}_s)) - 0.0114 \cdot (0.0317 + \tilde{c}_s)^{-1}$	[27]
$U_{\text{OCV},c} = -2.46444 \cdot \tilde{c}_s^6 + 2.20077 \cdot \tilde{c}_s^5 + 3.32765 \cdot \tilde{c}_s^4 - 5.71320 \cdot \tilde{c}_s^3 + 3.91673 \cdot \tilde{c}_s^2 - 2.09035 \cdot \tilde{c}_s + 4.19975 \cdot \exp(-0.03988 \cdot \tilde{c}_s^{414.66769}) + 0.18614$	[27]

Table A4. Identified parameter values in the full cell parameter study for highest volumetric capacity for discharge at 1C. The five best cell configurations, including the best-in-class configurations that were visualized with bar plots before, are shown along with their respective performance in all four investigated operating modes.

Parameters and performance	#1	#2	#3	#4	#5
$\varepsilon_a^{\text{CC}}$ [-]	0.65	0.65	0.65	0.65	0.55
$\varepsilon_a^{\text{SEP}}$ [-]	0.55	0.55	0.55	0.55	0.55
$\varepsilon_c^{\text{SEP}}$ [-]	0.45	0.45	0.45	0.45	0.45
$\varepsilon_c^{\text{CC}}$ [-]	0.55	0.55	0.55	0.55	0.55
R_a^{CC} [μm]	3	3	3	3	3
R_a^{SEP} [μm]	9	9	9	9	9
R_c^{SEP} [μm]	3	3	9	9	9
R_c^{CC} [μm]	3	9	3	9	9
\tilde{C}_a^{CC} [%]	75	75	75	75	75
\tilde{C}_c^{CC} [%]	25	25	25	25	25

Table A4. Continued.

Parameters and performance	#1	#2	#3	#4	#5
Vol. capacity 0.1C discharge [mAh cm ⁻³]	146.36	146.35	146.35	146.35	138.86
Vol. capacity 0.1C charge [mAh cm ⁻³]	140.55	140.55	140.56	140.56	134.23
Vol. capacity 1C discharge [mAh cm ⁻³]	134.39	134.38	134.36	134.36	132.79
Vol. capacity 1C charge [mAh cm ⁻³]	66.56	66.57	66.57	66.58	96.01

Table A5. Identified parameter values in the full cell parameter study for highest volumetric capacity for charge at 1C. The five best cell configurations, including the best-in-class configurations that were visualized with bar plots before, are shown along with their respective performance in all four investigated operating modes.

Parameters and performance	#1	#2	#3	#4	#5
ϵ_a^{cc} [-]	0.45	0.45	0.45	0.45	0.55
ϵ_a^{sep} [-]	0.45	0.45	0.45	0.45	0.45
ϵ_c^{sep} [-]	0.45	0.45	0.45	0.45	0.45
ϵ_c^{cc} [-]	0.55	0.55	0.55	0.55	0.55
R_a^{cc} [μ m]	3	3	3	3	3
R_a^{sep} [μ m]	9	9	9	9	9
R_c^{sep} [μ m]	9	3	9	3	3
R_c^{cc} [μ m]	9	9	3	3	3
\tilde{C}_a^{cc} [%]	75	75	75	75	75
\tilde{C}_c^{cc} [%]	75	75	75	75	25
Vol. capacity 0.1C discharge [mAh cm ⁻³]	131.61	131.61	131.62	131.62	135.53
Vol. capacity 0.1C charge [mAh cm ⁻³]	128.01	128.01	128.01	128.01	131.45
Vol. capacity 1C discharge [mAh cm ⁻³]	88.94	90.54	88.99	90.57	122.51
Vol. capacity 1C charge [mAh cm ⁻³]	100.62	100.62	100.62	100.61	98.29

Acknowledgements

This work was financially supported by the BMBF within the HighEnergy project and the HiStructures project under grant numbers 03XP0073A and 03XP0243B, respectively.

Open access funding enabled and organized by Projekt DEAL.

Conflict of Interest

The authors declare no conflict of interest.

Keywords

design guidelines, multilayered electrodes, pseudo-2D model, parameter screening

Received: November 11, 2020

Revised: January 17, 2021

Published online:

- [1] A. W. Schäfer, S. R. H. Barrett, K. Doyme, L. M. Dray, A. R. Gnad, R. Self, A. O'Sullivan, A. P. Synodinos, A. J. Torija, *Nat. Energy* **2019**, *4*, 160.

- [2] D. L. Wood, M. Wood, J. Li, Z. Du, R. E. Ruther, K. A. Hays, N. Muralidharan, L. Geng, C. Mao, I. Belharouak, *Energy Storage Mater.* **2020**, *29*, 254.
- [3] A. Kwade, W. Haselrieder, R. Leithoff, A. Modlinger, F. Dietrich, K. Droeder, *Nat. Energy* **2018**, *3*, 290.
- [4] S. Ahmed, I. Bloom, A. N. Jansen, T. Tanim, E. J. Dufek, A. Pesaran, A. Burnham, R. B. Carlson, F. Dias, K. Hardy, M. Keyser, C. Kreuzer, A. Markel, A. Meintz, C. Michelbacher, M. Mohanpurkar, P. A. Nelson, D. C. Robertson, D. Scofield, M. Shirk, T. Stephens, R. Vijayagopal, J. Zhang, *J. Power Sources* **2017**, *367*, 250.
- [5] W. Xie, X. Liu, R. He, Y. Li, X. Gao, X. Li, Z. Peng, S. Feng, X. Feng, S. Yang, *J. Energy Storage* **2020**, *32*, 101837.
- [6] T. Waldmann, B. I. Hogg, M. Wohlfahrt-Mehrens, *J. Power Sources* **2018**, *384*, 107.
- [7] Y. Liu, Y. Zhu, Y. Cui, *Nat. Energy* **2019**, *4*, 540.
- [8] A. M. Colclasure, A. R. Dunlop, S. E. Trask, B. J. Polzin, A. N. Jansen, K. Smith, *J. Electrochem. Soc.* **2019**, *166*, A1412.
- [9] E. Logan, J. Dahn, *Trends Chem.* **2020**, *2*, 354.
- [10] N. Kim, S. Chae, J. Ma, M. Ko, J. Cho, *Nat. Commun.* **2017**, *8*, 1.
- [11] A. Tomaszewska, Z. Chu, X. Feng, S. O'Kane, X. Liu, J. Chen, C. Ji, E. Endler, R. Li, L. Liu, Y. Li, S. Zheng, S. Vetterlein, M. Gao, J. Du, M. Parkes, M. Ouyang, M. Marinescu, G. Offer, B. Wu, *eTransportation* **2019**, *1*, 100011.
- [12] P. M. Attia, A. Grover, N. Jin, K. A. Severson, T. M. Markov, Y. H. Liao, M. H. Chen, B. Cheong, N. Perkins, Z. Yang, P. K. Herring, M. Aykol,

- S. J. Harris, R. D. Braatz, S. Ermon, W. C. Chueh, *Nature* **2020**, 578, 397.
- [13] M. Xu, R. Wang, B. Reichman, X. Wang, *J. Energy Storage* **2018**, 20, 298.
- [14] M. Torchio, L. Magni, R. Braatz, D. Raimondo, *IFAC-PapersOnLine* **2016**, 49, 827.
- [15] T. R. Tanim, E. J. Dufek, M. Evans, C. Dickerson, A. N. Jansen, B. J. Polzin, A. R. Dunlop, S. E. Trask, R. Jackman, I. Bloom, Z. Yang, E. Lee, *J. Electrochem. Soc.* **2019**, 166, A1926.
- [16] S. Schindler, M. Bauer, H. Cheetamun, M. A. Danzer, *J. Energy Storage* **2018**, 19, 364.
- [17] H. Wang, S. Frisco, E. Gottlieb, R. Yuan, J. F. Whitacre, *J. Power Sources* **2019**, 426, 67.
- [18] C. Mao, R. E. Ruther, J. Li, Z. Du, I. Belharouak, *Electrochem. Commun.* **2018**, 97, 37.
- [19] X. G. Yang, G. Zhang, S. Ge, C. Y. Wang, *Proc. Natl. Acad. Sci. U.S.A.* **2018**, 115, 7266.
- [20] X. G. Yang, T. Liu, Y. Gao, S. Ge, Y. Leng, D. Wang, C. Y. Wang, *Joule* **2019**, 3, 3002.
- [21] B. S. Vishnugopi, A. Verma, P. P. Mukherjee, *J. Electrochem. Soc.* **2020**, 167, 090508.
- [22] L. S. Kremer, A. Hoffmann, T. Danner, S. Hein, B. Prifling, D. Westhoff, C. Dreer, A. Latz, V. Schmidt, M. Wohlfahrt-Mehrens, *Energy Technol.* **2020**, 8, 1900167.
- [23] H. Buqa, D. Goers, M. Holzapfel, M. E. Spahr, P. Novák, *J. Electrochem. Soc.* **2005**, 152, A474.
- [24] D. Schmidt, M. Kamlah, V. Knoblauch, *J. Energy Storage* **2018**, 17, 213.
- [25] R. Darling, *J. Electrochem. Soc.* **1997**, 144, 4201.
- [26] Y. Liu, H. Liu, X. Zhao, L. Wang, G. Liang, *J. Wuhan Univ. Technol.-Mater. Sci. Ed.* **2019**, 34, 549.
- [27] V. Laue, F. Röder, U. Krewer, *Electrochim. Acta* **2019**, 314, 20.
- [28] F. Röder, S. Sonntag, D. Schröder, U. Krewer, *Energy Technol.* **2016**, 4, 1588.
- [29] L. Bläubaum, F. Röder, C. Nowak, H. S. Chan, A. Kwade, U. Krewer, *ChemElectroChem* **2020**, 7, 4755.
- [30] S. Yu, S. Kim, T. Y. Kim, J. H. Nam, W. I. Cho, *Bull. Korean Chem. Soc.* **2013**, 34, 79.
- [31] J. B. Hadedank, J. Endres, P. Schmitz, M. F. Zaeh, H. P. Huber, *J. Laser Appl.* **2018**, 30, 32205.
- [32] P. Smyrek, J. Pröll, H. J. Seifert, W. Pfleging, *J. Electrochem. Soc.* **2015**, 163, A19.
- [33] M. Mangang, H. J. Seifert, W. Pfleging, *J. Power Sources* **2016**, 304, 24.
- [34] J. Pröll, H. Kim, A. Piqué, H. J. Seifert, W. Pfleging, *J. Power Sources* **2014**, 255, 116.
- [35] S. Golmon, K. Maute, M. L. Dunn, *J. Power Sources* **2014**, 253, 239.
- [36] A. Yao, J. Hwang, (EnPower, Inc.), *US 2020/0212437 A1*, **2020**.
- [37] D. Westhoff, T. Danner, S. Hein, R. Scurtu, L. Kremer, A. Hoffmann, A. Hilger, I. Manke, M. Wohlfahrt-Mehrens, A. Latz, V. Schmidt, *Mater. Charact.* **2019**, 151, 166.
- [38] Y. Qi, T. Jang, V. Ramadesigan, D. T. Schwartz, V. R. Subramanian, *J. Electrochem. Soc.* **2017**, 164, A3196.
- [39] J. Christensen, V. Srinivasan, J. Newman, *J. Electrochem. Soc.* **2006**, 153, A560.
- [40] V. Ramadesigan, R. N. Methekar, F. Latinwo, R. D. Braatz, V. R. Subramanian, *J. Electrochem. Soc.* **2010**, 157, A1328.
- [41] Y. H. Chen, C. W. Wang, X. Zhang, A. M. Sastry, *J. Power Sources* **2010**, 195, 2851.
- [42] Y. Dai, V. Srinivasan, *J. Electrochem. Soc.* **2016**, 163, A406.
- [43] S. De, P. W. Northrop, V. Ramadesigan, V. R. Subramanian, *J. Power Sources* **2013**, 227, 161.
- [44] A. J. Salkind, C. Fennie, P. Singh, T. Atwater, D. E. Reisner, *J. Power Sources* **1999**, 80, 293.
- [45] M. W. Verbrugge, R. S. Conell, *J. Electrochem. Soc.* **2002**, 149, A45.
- [46] S. G. Marquis, V. Sulzer, R. Timms, C. P. Please, S. J. Chapman, *J. Electrochem. Soc.* **2019**, 166, A3693.
- [47] M. Doyle, T. F. Fuller, J. Newman, *J. Electrochem. Soc.* **1993**, 140, 1526.
- [48] G. S. Nagarajan, J. W. Van Zee, R. M. Spotnitz, *J. Electrochem. Soc.* **1998**, 145, 771.
- [49] M. Meyer, L. Komsysiaka, B. Lenz, C. Agert, *Appl. Math. Model.* **2013**, 37, 2016.
- [50] S. T. Taleghani, B. Marcos, K. Zaghbi, G. Lantagne, *J. Electrochem. Soc.* **2019**, 166, A225.
- [51] S. Golmon, K. Maute, M. L. Dunn, *Int. J. Numer. Meth. Eng.* **2012**, 92, 475.
- [52] N. Lin, X. Xie, R. Schenkendorf, U. Krewer, *J. Electrochem. Soc.* **2018**, 165, A1169.
- [53] S. Hein, J. Feinauer, D. Westhoff, I. Manke, V. Schmidt, A. Latz, *J. Power Sources* **2016**, 336, 161.
- [54] D. Westhoff, I. Manke, V. Schmidt, *Comput. Mater. Sci.* **2018**, 151, 53.
- [55] J. Joos, A. Buchele, A. Schmidt, A. Weber, E. Ivers-Tiffée, *Energy Technol.* **2021**, 2000891.
- [56] P. R. Shearing, L. E. Howard, P. S. Jørgensen, N. P. Brandon, S. J. Harris, *Electrochem. Commun.* **2010**, 12, 374.
- [57] M. Ender, J. Joos, A. Weber, E. Ivers-Tiffée, *J. Power Sources* **2014**, 269, 912.
- [58] S. Komini Babu, A. I. Mohamed, J. F. Whitacre, S. Litster, *J. Power Sources* **2015**, 283, 314.
- [59] M. Ender, J. Joos, T. Carraro, E. Ivers-Tiffée, *Electrochem. Commun.* **2011**, 13, 166.
- [60] J. R. Wilson, J. S. Cronin, S. A. Barnett, S. J. Harris, *J. Power Sources* **2011**, 196, 3443.
- [61] L. Zielke, T. Hutzenlaub, D. R. Wheeler, C. W. Chao, I. Manke, A. Hilger, N. Paust, R. Zengerle, S. Thiele, *Adv. Energy Mater.* **2015**, 5, 1.
- [62] M. Ender, J. Joos, T. Carraro, E. Ivers-Tiffée, *J. Electrochem. Soc.* **2012**, 159, A972.
- [63] L. Almar, J. Joos, A. Weber, E. Ivers-Tiffée, *J. Power Sources* **2019**, 427, 1.
- [64] A. Latz, J. Zausch, *J. Power Sources* **2011**, 196, 3296.
- [65] S. Hein, T. Danner, A. Latz, *ACS Appl. Energy Mater.* **2020**, 3, 8519.
- [66] A. Mistry, F. L. E. Usseglio-Viretta, A. Colclasure, K. Smith, P. P. Mukherjee, *J. Electrochem. Soc.* **2020**, 167, 090542.
- [67] M. Kespe, M. Gleiß, S. Hammerich, H. Nirschl, *Int. J. Energy Res.* **2017**, 41, 2282.
- [68] M. Chouchane, A. Rucci, T. Lombardo, A. C. Ngandjong, A. A. Franco, *J. Power Sources* **2019**, 444, 227285.
- [69] M. Duquesnoy, T. Lombardo, M. Chouchane, E. N. Primo, A. A. Franco, *J. Power Sources* **2020**, 480, 229103.
- [70] S. L. Mitchell, M. Ortiz, *J. Power Sources* **2016**, 326, 242.
- [71] A. N. Mistry, K. Smith, P. P. Mukherjee, *ACS Appl. Mater. Interfaces* **2018**, 10, 6317.
- [72] V. Laue, N. Wolff, F. Röder, U. Krewer, *Energy Technol.* **2020**, 8, 1801049.
- [73] I. S. Sarpal, A. Bensmann, J. Mähliß, D. Hennefeld, R. Hanke-Rauschenbach, *Int. J. Electr. Power Energy Syst.* **2018**, 99, 722.
- [74] M. W. Hermanto, N. C. Kee, R. B. H. Tan, M.-S. Chiu, R. D. Braatz, *AIChE J.* **2008**, 54, 3248.
- [75] L. Su, J. Zhang, C. Wang, Y. Zhang, Z. Li, Y. Song, T. Jin, Z. Ma, *Appl. Energy* **2016**, 163, 201.
- [76] O. Rynne, M. Dubarry, C. Molson, D. Lepage, A. Prébé, D. Aymé-Perrot, D. Rochefort, M. Dollé, *Batteries* **2019**, 5, 72.
- [77] F. Galvanin, M. Barolo, F. Bezzo, *IFAC Proc.* **2010**, 43, 571.
- [78] A. Chakrabarty, G. T. Buzzard, A. E. Rundell, *Wiley Interdiscip. Rev.: Syst. Biol. Med.* **2013**, 5, 181.
- [79] F. Galvanin, C. C. Ballan, M. Barolo, F. Bezzo, *J. Pharmacokin. Pharmacodyn.* **2013**, 40, 451.

- [80] R. Schenkendorf, X. Xie, M. Rehbein, S. Scholl, U. Krewer, *Processes* **2018**, *6*, 27.
- [81] S. Curtarolo, G. L. Hart, M. B. Nardelli, N. Mingo, S. Sanvito, O. Levy, *Nat. Mater.* **2013**, *12*, 191.
- [82] J. E. Saal, S. Kirklín, M. Aykol, B. Meredig, C. Wolverton, *JOM* **2013**, *65*, 1501.
- [83] R. Xiao, H. Li, L. Chen, *Sci. Rep.* **2015**, *5*, 1.
- [84] W. Fitzhugh, F. Wu, L. Ye, W. Deng, P. Qi, X. Li, *Adv. Energy Mater.* **2019**, *9*, 1900807.
- [85] R. P. Cunha, T. Lombardo, E. N. Primo, A. A. Franco, *Batteries Supercaps* **2020**, *3*, 60.
- [86] K. A. Severson, P. M. Attia, N. Jin, N. Perkins, B. Jiang, Z. Yang, M. H. Chen, M. Aykol, P. K. Herring, D. Fraggedakis, M. Z. Bazant, S. J. Harris, W. C. Chueh, R. D. Braatz, *Nat. Energy* **2019**, *4*, 383.
- [87] A. Turetskyy, V. Laue, R. Lamprecht, S. Thiede, U. Krewer, C. Herrmann, in *2019 IEEE 17th Int. Conf. on Industrial Informatics (INDIN)*, IEEE **2019**, p. 53.
- [88] N. Dawson-Elli, S. B. Lee, M. Pathak, K. Mitra, V. R. Subramanian, *J. Electrochem. Soc.* **2018**, *165*, A1.
- [89] O. Schmidt, M. Thomitzek, F. Röder, S. Thiede, C. Herrmann, U. Krewer, *J. Electrochem. Soc.* **2020**, *167*, 060501.
- [90] V. Laue, O. Schmidt, H. Dreger, X. Xie, F. Röder, R. Schenkendorf, A. Kwade, U. Krewer, *Energy Technol.* **2019**, *8*, 1900201.
- [91] X. Xie, R. Schenkendorf, U. Krewer, *Processes* **2018**, *6*, 1.
- [92] X. Xie, R. Schenkendorf, *Chem. Eng. Sci.* **2019**, *207*, 805.
- [93] M. Doyle, J. Newman, *Electrochim. Acta* **1995**, *40*, 2191.
- [94] N. Legrand, S. Raël, B. Knosp, M. Hinaje, P. Desprez, F. Lapique, *J. Power Sources* **2014**, *251*, 370.
- [95] B. Tjaden, S. J. Cooper, D. J. Brett, D. Kramer, P. R. Shearing, *Curr. Opin. Chem. Eng.* **2016**, *12*, 44.
- [96] J. Landesfeind, H. A. Gasteiger, *J. Electrochem. Soc.* **2019**, *166*, A3079.
- [97] C. Sangrós Giménez, B. Finke, C. Nowak, C. Schilde, A. Kwade, *Adv. Powder Technol.* **2018**, *29*, 2312.
- [98] A. A. Tahmasbi, T. Kadyk, M. H. Eikerling, *J. Electrochem. Soc.* **2017**, *164*, A1307.
- [99] F. M. Kindermann, J. Keil, A. Frank, A. Jossen, *J. Electrochem. Soc.* **2017**, *164*, E287.
- [100] A. Tahmasbi, M. Eikerling, *Electrochim. Acta* **2018**, *283*, 75.
- [101] H. Bockholt, M. Indrikova, A. Netz, F. Golks, A. Kwade, *J. Power Sources* **2016**, *325*, 140.
- [102] Z. Du, D. L. Wood, C. Daniel, S. Kalnaus, J. Li, *J. Appl. Electrochem.* **2017**, *47*, 405.
- [103] R. Wang, Sankey Diagram, <https://www.mathworks.com/matlabcentral/fileexchange/75813-sankey-diagram> (accessed: September 2020).



Daniel Witt received his bachelor's degree from University of Paderborn (Germany) in Chemical Engineering in 2016 and a master's degree with honors from TU Braunschweig (Germany) in Biochemical and Chemical Engineering in 2018. During his master's, he worked on the model-based proton-exchange membrane fuel cell diagnosis in the research group of Professor M. Eikerling (Simon Fraser University, Canada). Since 2019, he has been pursuing his Ph.D. under supervision of Professor U. Krewer at Karlsruhe Institute of Technology. His research focuses on model-based diagnostics for electrochemical systems with emphasis on better understanding and eventually optimization of cell design, production, and degradation.



Ulrike Krewer is full professor and director of the Institute of Applied Materials–Electrochemical Technologies, at Karlsruhe Institute of Technology. After a Ph.D. in 2005 at the Max Planck Institute Magdeburg, a 2-year research stay at Samsung (Korea), and a junior research group in Magdeburg, she was full professor at TU Braunschweig, visiting scholar at MIT, and board member of the Battery LabFactory Braunschweig until 2020. She has been active for 20 years in the field of dynamic and model-based analysis and optimization of electrodes and cells, comprising low-temperature fuel cells, Li(-ion) batteries, electrolysis, and electrosynthesis.